# UNIVERSIDAD DE CONCEPCIÓN



## Centro de Investigación en Ingeniería Matemática (CI$^2$MA)




**A hybridizable discontinuous Galerkin method for the time-dependent eddy current problem in an electric field formulation**

Ramiro Acevedo, Rommel Bustinza,
Christian Gómez

PREPRINT 2026-36

SERIE DE PRE-PUBLICACIONES

# A hybridizable discontinuous Galerkin method for the time-dependent eddy current problem in an electric field formulation

Ramiro Acevedo[1], Rommel Bustinza[2,3], and Christian Gómez[4]

[1]Corresponding author. Departamento de Matemáticas, Universidad del Cauca, Popayán, Colombia
e-mail: rmacevedo@unicauca.edu.co, ORCID: 0000-0002-6844-5992
[2]Departamento de Ingeniería Matemática, Universidad de Concepción, Concepción, Chile.
[3]Centro de Investigación en Ingeniería Matemática, CI[2]MA, Concepción, Chile.
e-mail: rbustinza@udec.cl, ORCID: 0000-0001-6355-8341
[4]Departamento de Matemáticas y Física, Universidad de los Llanos, Villavicencio, Colombia.
e-mail: chgomez@unillanos.edu.co, ORCID: 0000-0002-7311-8478

**Abstract**

In this work we propose and analyze a hybridizable discontinuous Galerkin (HDG) method for the time-dependent eddy current problem in an electric field formulation, posed in a domain consisting of a conductor and a dielectric region. The divergence-free condition in the dielectric and the zero-flux condition on the interface between both media are imposed by means of a Lagrange multiplier. The flux condition only adds one global scalar unknown, so that the static condensation remains local. The time discretization is performed with the backward Euler scheme. We prove that the fully discrete problem is well posed and derive error estimates of order $\mathcal{O}(h^{k+1/2} + \Delta t)$ for polynomial degree $k \geq 0$. To the best of our knowledge, these are the first error estimates for an HDG method applied to the transient eddy current problem. Numerical experiments show first order in $\Delta t$ and, for $k = 0, 1, 2$, computed spatial orders are better than the proved ones. Moreover, we illustrate the robustness of the method on a model problem of magnetic shielding by eddy currents.

**Mathematics Subject Classifications (1991)**: 65M60, 65N15; 65M12, 35Q61, 35K65; 78M10

**Key words**: Eddy current problem, hybridizable discontinuous Galerkin method, degenerate parabolic problem, backward Euler scheme, error estimates.

## 1 Introduction

The problem that motivates this work is that of a conductor in contact with a dielectric material. An imposed current density, with a general time dependence, flows in the dielectric and induces currents in the conductor. When the fields vary slowly, the displacement current can be neglected in the Ampère–Maxwell law, and the electromagnetic field is governed by the eddy current model (eddy currents are also known as Foucault currents). The model and its analysis are presented in the monographs [7, 11, 13]. Ammari, Buffa, and Nédélec [8] proved that the eddy current model approximates the Maxwell equations at low frequencies.

In the time-harmonic regime, the approximation is of second order in the frequency if the source current of the problem satisfies an additional condition, and of first order otherwise, and the results depend on the topology of the domain. They also studied the time-dependent case. When the source has a general time dependence, the model does not reduce to a time-harmonic problem, and an evolution problem has to be solved to describe the transient regime from a given initial state.

When the computational domain contains a dielectric region in addition to the conductor, the conductivity vanishes in that region. The transient problem is then parabolic in the conductor and, at each time instant, elliptic in the dielectric, that is, degenerate parabolic. This problem has been studied with conforming finite elements in several formulations. For formulations in terms of the magnetic field, a magnetic scalar potential has been used in the dielectric [32], and the constraint that the field satisfies there has been imposed with a Lagrange multiplier, either in a formulation coupled with boundary elements [26] or in a saddle point formulation [1]. The problem has been analyzed with current intensities as data in [12]. In that work and in [1], error estimates have been proved for fully discrete schemes based on Nédélec elements and the backward Euler method.

In formulations based on the electric field or on its time primitive, the equation loses its evolution term in the dielectric, and the electric field is determined there only if two constraints are imposed. The electric displacement $\varepsilon\mathbf{E}$ must be divergence free in the dielectric, and its total flux through the interface with the conductor must vanish. The second constraint, the charge condition, states that the conductor has no net charge. The problem has been analyzed in [4, 5] with a time primitive of the electric field as the unknown and a Lagrange multiplier for the divergence constraint, and [3] provides a fully discrete abstract framework for a family of mixed degenerate parabolic problems that includes the formulation of [5]. More recently, Šebestová [31] obtained a residual-based a posteriori error estimate for an electric field-based formulation, also with Nédélec elements and the backward Euler method.

Unlike conforming finite elements, discontinuous Galerkin (DG) methods do not require continuity of the approximation across elements, which gives flexibility in the choice of meshes and polynomial degrees. Perugia and Schötzau [28] analyzed an *hp*-local DG method, formulated in terms of the electric field, for the low-frequency time-harmonic Maxwell equations in heterogeneous media with conducting and insulating materials. For the time-harmonic eddy current problem in terms of the magnetic field, Alonso Rodríguez, Márquez, Meddahi, and Valli [6] analyzed a DG method that uses a magnetic scalar potential in the insulator. The price of the discontinuity across elements is the size of the global system, which contains the volume degrees of freedom of all the elements, and these are more numerous than those of a conforming method of the same degree. Hybridizable discontinuous Galerkin (HDG) methods [20] retain the discontinuous character of the approximation and allow the interior variables to be eliminated element by element, so that the only globally coupled degrees of freedom are those of the numerical traces on the faces of the mesh. Their a priori analysis usually relies on projections tailored to the form of the numerical traces [21].

Nguyen, Peraire, and Cockburn [27] proposed HDG methods for the time-harmonic Maxwell equations, one of them with a Lagrange multiplier for the divergence-free condition, and studied them numerically. Later, a superconvergent HDG method with a multiplier was analyzed for the stationary Maxwell equations [16]. For eddy currents, Bustinza, López-Rodríguez, and Osorio [14] analyzed an HDG method for the time-harmonic problem in a domain with a conductor and a dielectric. That method uses a multiplier in the dielectric and the tangential and normal traces of the electric field, and it incorporates the charge condition on the interface. The authors obtained a priori error estimates of order $\mathcal{O}(h^{k+1/2})$.

HDG methods have also been analyzed for evolution problems. For instance, for scalar parabolic equations, where uniform-in-time superconvergence has been established for the semidiscretization of the heat

equation [15] and a fully discrete analysis with the backward Euler method is known for convection-diffusion-reaction equations [29]. For the time-dependent Maxwell equations, Christophe, Descombes, and Lanteri [17] presented a three-dimensional implicit HDG method and studied it numerically. Berardocco, Kronbichler, and Gravemeier [10] proposed two HDG schemes with a conductivity term: one for the Maxwell equations in mixed form, which retains the displacement current, and another for the electromagnetic diffusion equation in terms of the electric field, which omits it. Their numerical examples use the former. Unlike these works, which study their methods only numerically, Cockburn, Du, and Sánchez [19] carried out an a priori error analysis of a class of semidiscrete Hamiltonian HDG methods, and Lee [25] obtained error bounds in space and time for an HDG method in time-modulated Drude–Lorentz media, in both cases for the full Maxwell equations. To the best of our knowledge, the only error analysis of an HDG method for eddy currents is that of [14], for the time-harmonic regime, whereas no estimates are available for the transient one.

In this work, we propose and analyze a fully discrete HDG method for the transient eddy current problem formulated in terms of the electric field, in a bounded domain that contains a conductor and a dielectric region. As in the time-harmonic method in [14], a Lagrange multiplier is introduced in the dielectric. The unknowns are the electric field $\boldsymbol{u} = \mathbf{E}$, the variable $\boldsymbol{z} = \mu^{-1}\,\mathbf{curl}\,\boldsymbol{u}$, and the multiplier $\varphi$, together with the tangential trace of the electric field on all faces of the mesh and the trace of the multiplier on the faces of the elements in the dielectric. All of them are approximated by polynomials of the same degree $k$. The multiplier is associated with the divergence constraint, written as $\operatorname{div}(\varepsilon\boldsymbol{u}) = \varphi$, and vanishes for the exact solution. On the interface, the trace of the multiplier is a single unknown constant. The charge condition, that is, the zero-flux condition on the interface, is thus imposed without penalty parameters and adds only one global scalar unknown, so that static condensation remains local. We discretize in time with the backward Euler method. We work with the electric field, as in [14], rather than with its time primitive, which is the unknown in [4, 5], at the cost of taking the time derivative of the current density as data. In a previous paper [2], the authors treated the same phenomenon, with current intensities as the excitation, using a formulation in terms of potentials and nodal finite elements.

We establish that the fully discrete scheme has a unique solution at each time step and, for homogeneous boundary data, satisfies a discrete energy estimate with a constant independent of $h$ and $\Delta t$. If the exact solution is piecewise regular enough, the source is sufficiently regular in time, the stabilization parameters are of order one, and $\Delta t \le 1/2$, the error is of order $\mathcal{O}(h^{k+1/2} + \Delta t)$ for the electric field in $\ell^\infty(L^2)$ on the conductor, and for $\boldsymbol{z}$ and the multiplier in $\ell^2(L^2)$. In space, this is the same order as that obtained in [14] for the time-harmonic regime. The analysis combines a discrete energy argument for the time derivative term $\sigma\partial_t\boldsymbol{u}$, which acts only in the conductor, with a discrete integration-by-parts formula that moves the curl from the source term onto $\boldsymbol{z}$ and onto the stabilization term. Instead of projections tailored to the numerical traces, the analysis uses $L^2$ projections onto the elements and the faces of the mesh. Some face terms do not vanish for these projections, and the estimate is suboptimal by $h^{1/2}$ in space.

In experiments with manufactured solutions the scheme is of first order in $\Delta t$ when the temporal part of the error dominates. The spatial part of the error decreases with orders above those of the estimate, close to $k+1$ for $k = 1, 2$, and approaching or exceeding 1 for $k = 0$. A model problem of magnetic shielding by eddy currents illustrates the method in a configuration of physical interest. No numerical results are reported in [14]. Our scheme differs from that method in the time dependence and in the treatment of the charge condition, but both use the same Lagrange multiplier in the dielectric and the tangential trace of the electric field as an unknown on the faces. The experiments of Section 5 thus complement the analysis of [14] with numerical evidence on the behavior of these two ingredients.

IThe rest of the paper is organized as follows. We present the model, its first-order system, and its

variational formulation in Section 2, where we show that the multiplier vanishes. In Section 3 we introduce the HDG method and prove that the fully discrete scheme has a unique solution and is stable. Section 4 contains the a priori error analysis. Finally, in Section 5 we present some numerical experiments, that validate our theoretical findings.

## 2 Eddy current problem

Maxwell's equations are used to describe electromagnetic phenomena. The eddy current model results by disregarding the displacement current in the Ampère–Maxwell law [13]. Let $\Omega$ be a bounded, simply connected polyhedral domain with connected Lipschitz boundary $\Gamma := \partial\Omega$. We denote by $\Omega_{\mathtt{c}}$ and $\Omega_{\mathtt{d}}$ the conducting and dielectric regions in $\Omega$: $\Omega_{\mathtt{c}}$ is a connected Lipschitz polyhedron with $\overline{\Omega_{\mathtt{c}}} \subset \Omega$ and connected boundary $\Gamma_0 := \partial\Omega_{\mathtt{c}}$, and $\Omega_{\mathtt{d}} := \Omega \setminus \Omega_{\mathtt{c}}$, which we assume connected. Thus $\overline{\Omega} = \overline{\Omega_{\mathtt{c}}} \cup \overline{\Omega_{\mathtt{d}}}$ and $\partial\Omega_{\mathtt{d}} = \Gamma \cup \Gamma_0$. The problem consists in determining the electric field $\mathbf{E}(t, \boldsymbol{x})$ and the magnetic field $\mathbf{H}(t, \boldsymbol{x})$ satisfying

$$\begin{aligned} \mathbf{curl}\,\mathbf{H} - \sigma\mathbf{E} &= \mathbf{J} \quad \text{in } \Omega, \\ \partial_t(\mu\mathbf{H}) + \mathbf{curl}\,\mathbf{E} &= 0 \quad \text{in } \Omega, \\ \operatorname{div}(\varepsilon\mathbf{E}) &= 0 \quad \text{in } \Omega_{\mathtt{d}}, \end{aligned} \tag{1}$$

where $\mathbf{J}(t, \boldsymbol{x})$ is the current density source. The electromagnetic coefficients are time-independent: magnetic permeability $\mu$, electric permittivity $\varepsilon$, and electric conductivity $\sigma$. We assume

$$\begin{aligned} 0 < \underline{\mu} \le \mu(\boldsymbol{x}) \le \overline{\mu} \quad \text{in } \Omega, \quad 0 < \underline{\varepsilon} \le \varepsilon(\boldsymbol{x}) \le \overline{\varepsilon} \quad \text{in } \Omega, \\ 0 < \underline{\sigma} \le \sigma(\boldsymbol{x}) \le \overline{\sigma} \quad \text{in } \Omega_{\mathtt{c}}, \qquad \sigma(\boldsymbol{x}) = 0 \text{ in } \Omega_{\mathtt{d}}, \end{aligned} \tag{2}$$

and that $\mu$, $\varepsilon$ and $\sigma$ are piecewise constant on a finite polyhedral partition of $\overline{\Omega}$. For the source, we assume that $\mathbf{J} = \mathbf{curl}\,\mathbf{H}_{\mathtt{s}}$, where $\mathbf{H}_{\mathtt{s}} \in H^1(0, T; [H^1(\Omega)]^3)$ is a given magnetic field source (for instance, the field generated by a coil). In particular, $\mathbf{J}$ is divergence-free.

The equations (1) are completed with the conditions

$$\begin{aligned} \int_{\Gamma_0} \varepsilon\mathbf{E}|_{\Omega_{\mathtt{d}}} \cdot \boldsymbol{n}_0 = 0, \\ \boldsymbol{n} \times \mathbf{E} = \boldsymbol{g} \qquad \text{on } \Gamma, \\ \mathbf{E}(0, \cdot) = \boldsymbol{u}_0(\cdot) \qquad \text{in } \Omega_{\mathtt{c}}, \end{aligned} \tag{3}$$

where $\boldsymbol{n}$ denotes the unit outward normal vector to $\Gamma$, and $\boldsymbol{n}_0$ the unit normal vector on $\Gamma_0$ pointing outward from $\Omega_{\mathtt{d}}$. Furthermore, $\boldsymbol{g}$ and $\boldsymbol{u}_0$ represent given data. The initial condition is only prescribed in $\Omega_{\mathtt{c}}$, since there is no time derivative of $\mathbf{E}$ in $\Omega_{\mathtt{d}}$.

Differentiating the first equation in (1) with respect to time and using the second one, we obtain the curl–curl evolution equation

$$\sigma\partial_t\mathbf{E} + \mathbf{curl}(\mu^{-1}\,\mathbf{curl}\,\mathbf{E}) = -\partial_t\mathbf{J} \qquad \text{in } \Omega.$$

Introducing

$$\boldsymbol{u} = \mathbf{E}, \qquad \boldsymbol{z} = \mu^{-1}\,\mathbf{curl}\,\boldsymbol{u},$$

and a Lagrange multiplier $\varphi$ in $\Omega_{\mathtt{d}}$, we arrive at the first-order system

$$\begin{aligned}
\mu \boldsymbol{z} - \mathbf{curl}\, \boldsymbol{u} &= 0 && \text{in } \Omega,\\
\sigma \partial_t \boldsymbol{u} + \mathbf{curl}\, \boldsymbol{z} - \varepsilon \nabla \varphi|_{\Omega_{\mathtt{d}}} &= -\partial_t \mathbf{J} && \text{in } \Omega,\\
\operatorname{div}(\varepsilon \boldsymbol{u}) &= \varphi && \text{in } \Omega_{\mathtt{d}},\\
\langle \varepsilon \boldsymbol{u}|_{\Omega_{\mathtt{d}}} \cdot \boldsymbol{n}_0, 1 \rangle_{\Gamma_0} &= 0, &&\\
\boldsymbol{n} \times \boldsymbol{u} &= \boldsymbol{g} && \text{on } \Gamma,\\
\varphi &= 0 && \text{on } \Gamma,\\
\varphi|_{\Gamma_0} &\in \mathbb{R}, &&\\
\boldsymbol{u}(0,\cdot) &= \boldsymbol{u}_0(\cdot) && \text{in } \Omega_{\mathtt{c}},
\end{aligned} \tag{4}$$

where the constant value of $\varphi$ on $\Gamma_0$ is also an unknown. We show below that $\varphi \equiv 0$, so that (4) is equivalent to the eddy current model.

In order to derive a variational formulation of (4), we take $\boldsymbol{g} = \mathbf{0}$ for simplicity (the general case is reduced to this one by means of a lifting $\boldsymbol{u}_{\boldsymbol{g}} \in \mathbf{H}(\mathbf{curl}; \Omega)$ with $\boldsymbol{n} \times \boldsymbol{u}_{\boldsymbol{g}} = \boldsymbol{g}$ on $\Gamma$), and introduce the spaces

$$X := \mathbf{H}_0(\mathbf{curl}; \Omega), \qquad \Theta := \left\{ \psi \in H^1(\Omega_{\mathtt{d}}) : \ \psi|_{\Gamma} = 0, \ \ \psi|_{\Gamma_0} \in \mathbb{R} \right\}.$$

For $\psi \in \Theta$ we denote by $c_\psi$ its constant value on $\Gamma_0$. Testing the second equation of (4) with $\boldsymbol{v} \in X$, the third one with $\psi \in \Theta$, and integrating by parts, we arrive at the following problem.

**Problem 1** *Find $\boldsymbol{u} : [0,T] \to X$ and $\varphi : [0,T] \to \Theta$ such that, for a.e. $t \in (0,T)$,*

$$\begin{aligned}
\frac{d}{dt}(\sigma \boldsymbol{u}, \boldsymbol{v})_\Omega + (\mu^{-1} \mathbf{curl}\, \boldsymbol{u}, \mathbf{curl}\, \boldsymbol{v})_\Omega - (\varepsilon \nabla \varphi, \boldsymbol{v})_{\Omega_{\mathtt{d}}} &= -(\partial_t \mathbf{J}, \boldsymbol{v})_\Omega && \forall\, \boldsymbol{v} \in X,\\
(\varphi, \psi)_{\Omega_{\mathtt{d}}} + (\varepsilon \boldsymbol{u}, \nabla \psi)_{\Omega_{\mathtt{d}}} &= 0 && \forall\, \psi \in \Theta,
\end{aligned} \tag{5}$$

*and $\sigma \boldsymbol{u}(0) = \sigma \boldsymbol{u}_0$.*

The second equation of (5) encodes both the divergence constraint and the flux condition on $\Gamma_0$. Indeed, since $\psi = 0$ on $\Gamma$,

$$(\varepsilon \boldsymbol{u}, \nabla \psi)_{\Omega_{\mathtt{d}}} = -(\operatorname{div}(\varepsilon \boldsymbol{u}), \psi)_{\Omega_{\mathtt{d}}} + c_\psi \, \langle \varepsilon \boldsymbol{u} \cdot \boldsymbol{n}_0, 1 \rangle_{\Gamma_0} \qquad \forall\, \psi \in \Theta,$$

and then, taking first $\psi \in H^1_0(\Omega_{\mathtt{d}})$ and then $\psi \in \Theta$ with $c_\psi = 1$, the second equation of (5) is equivalent to $\operatorname{div}(\varepsilon \boldsymbol{u}) = \varphi$ in $\Omega_{\mathtt{d}}$ together with $\langle \varepsilon \boldsymbol{u} \cdot \boldsymbol{n}_0, 1 \rangle_{\Gamma_0} = 0$.

**Proposition 2** *If $(\boldsymbol{u}, \varphi)$ solves Problem 1, then $\varphi \equiv 0$. Consequently, $\operatorname{div}(\varepsilon \boldsymbol{u}) = 0$ in $\Omega_{\mathtt{d}}$ and $\langle \varepsilon \boldsymbol{u} \cdot \boldsymbol{n}_0, 1 \rangle_{\Gamma_0} = 0$.*

**Proof.** Let $\psi \in \Theta$ and let $\widetilde{\psi}$ be its extension by the constant $c_\psi$ to $\Omega_{\mathtt{c}}$. Then $\widetilde{\psi} \in H^1_0(\Omega)$, so that $\boldsymbol{v} := \nabla \widetilde{\psi} \in X$ and $\mathbf{curl}\, \boldsymbol{v} = \mathbf{0}$. Moreover, $\boldsymbol{v} = \mathbf{0}$ in $\Omega_{\mathtt{c}}$ and $\sigma = 0$ in $\Omega_{\mathtt{d}}$, so that $(\sigma \boldsymbol{u}, \boldsymbol{v})_\Omega = 0$, and $(\partial_t \mathbf{J}, \nabla \widetilde{\psi})_\Omega = (\mathbf{curl}\, \partial_t \mathbf{H}_{\mathtt{s}}, \nabla \widetilde{\psi})_\Omega = 0$. Testing the first equation of (5) with this $\boldsymbol{v}$, we obtain $(\varepsilon \nabla \varphi, \nabla \psi)_{\Omega_{\mathtt{d}}} = 0$ for all $\psi \in \Theta$. Taking $\psi = \varphi$ yields $\nabla \varphi = \mathbf{0}$ in $\Omega_{\mathtt{d}}$, and since $\varphi = 0$ on $\Gamma$ and $\Omega_{\mathtt{d}}$ is connected, $\varphi \equiv 0$. The last assertion follows from the equivalence stated above. □

As a consequence of Proposition 2, $\boldsymbol{u}$ is the time derivative of the solution of the **E**-based formulation of the eddy current problem analyzed in [5], to which we refer for existence and uniqueness results. In the sequel, $(\boldsymbol{z}, \boldsymbol{u}, \varphi) = (\mu^{-1} \mathbf{curl}\, \boldsymbol{u}, \boldsymbol{u}, 0)$ denotes the exact solution of (4).

# 3 The HDG method

## 3.1 Mesh notation and approximation spaces

Let $\mathcal{T}_h$ be a shape-regular simplicial partition of $\overline{\Omega}$, such that each element is contained either in $\overline{\Omega_{\mathtt{c}}}$ or in $\overline{\Omega_{\mathtt{d}}}$, and such that $\mu$, $\varepsilon$ and $\sigma$ are constant on each element. We let $h_K$ be the diameter of $K \in \mathcal{T}_h$ and $h := \max_{K\in\mathcal{T}_h} h_K$; without loss of generality, $h \le 1$. We write $\partial\mathcal{T}_h := \{\partial K : \ K \in \mathcal{T}_h\}$. The collection of all faces generated by the triangulation is denoted by $\mathcal{E}_h$. Among them, we distinguish the interior faces of the full mesh and the interior faces contained in the dielectric subdomain, namely $\mathcal{E}_h^I$ and $\mathcal{E}_h^{0,I}$, respectively. In addition, the sets of faces lying on $\Gamma$ and on the interface $\Gamma_0$ are denoted by $\mathcal{E}_h^\Gamma := \mathcal{E}_h \cap \Gamma$ and $\mathcal{E}_h^{\Gamma_0} := \mathcal{E}_h \cap \Gamma_0$, respectively. The meshes induced on $\overline{\Omega_{\mathtt{d}}}$ and $\overline{\Omega_{\mathtt{c}}}$ are denoted by $\mathcal{T}_h^d$ and $\mathcal{T}_h^c$, respectively. Their associated face sets are written as $\mathcal{E}_h^d$ and $\mathcal{E}_h^c$. For every element $K \in \mathcal{T}_h$, the symbol $\boldsymbol{n}$ stands for the unit outward normal vector on $\partial K$. Note that, for $K \in \mathcal{T}_h^d$ and a face $F \subset \partial K \cap \Gamma_0$, we have $\boldsymbol{n} = \boldsymbol{n}_0$ on $F$.

For any positive real number $s$, we introduce the broken Sobolev space

$$[H^s(\mathcal{T}_h)]^3 := \left\{ \mathbf{v} \in [L^2(\mathcal{T}_h)]^3 : \mathbf{v}|_K \in [H^s(K)]^3 \ \ \forall K \in \mathcal{T}_h \right\},$$

endowed with the broken seminorm $|\cdot|_{H^s(\mathcal{T}_h)}$.

Now let $\boldsymbol{w} \in [H^s(\mathcal{T}_h)]^3$ with $s > \frac{1}{2}$, and let $F$ be a face shared by two neighboring elements $K^+$ and $K^-$, that is, $F = \partial K^+ \cap \partial K^-$. We denote by $\boldsymbol{w}^\pm$ the traces of $\boldsymbol{w}$ on $F$ taken from the interior of $K^\pm$, and by $\boldsymbol{n}^\pm$ the corresponding outward unit normals. The jump of $\boldsymbol{w}$ across an interior face is defined by

$$[\![\boldsymbol{n} \odot \boldsymbol{w}]\!] := \boldsymbol{n}^+ \odot \boldsymbol{w}^+ + \boldsymbol{n}^- \odot \boldsymbol{w}^-,$$

where the symbol $\odot$ stands either for the scalar product $(\cdot)$ or for the vector product $(\times)$. If $F$ is a boundary face, we set

$$[\![\boldsymbol{n} \odot \boldsymbol{w}]\!] := \boldsymbol{n} \odot \boldsymbol{w},$$

where now $\boldsymbol{n}$ denotes the outward unit normal to $\Gamma$. For later use, we also split the trace of a vector field into tangential and normal components. More precisely,

$$\boldsymbol{w}^t := \boldsymbol{n} \times (\boldsymbol{w} \times \boldsymbol{n}), \qquad \boldsymbol{w}^n := (\boldsymbol{w} \cdot \boldsymbol{n})\boldsymbol{n},$$

so that

$$\boldsymbol{w} = \boldsymbol{w}^t + \boldsymbol{w}^n \qquad \text{on } \partial K.$$

We next introduce the elementwise and facewise inner products employed throughout the paper. For scalar functions $q, p$ we set

$$(q,p)_{\mathcal{T}_h} := \sum_{K\in\mathcal{T}_h} (q,p)_K, \qquad \langle q,p\rangle_{\partial\mathcal{T}_h} := \sum_{K\in\mathcal{T}_h} \langle q,p\rangle_{\partial K}.$$

For vector fields $\boldsymbol{v}, \boldsymbol{w}$, we define

$$(\boldsymbol{v},\boldsymbol{w})_{\mathcal{T}_h} := \sum_{j=1}^{3} (v_j, w_j)_{\mathcal{T}_h}, \qquad \langle \boldsymbol{v},\boldsymbol{w}\rangle_{\partial\mathcal{T}_h} := \sum_{j=1}^{3} \langle v_j, w_j\rangle_{\partial\mathcal{T}_h}.$$

Here,

$$(q,p)_K := \int_K q\,p, \qquad \langle q,p\rangle_{\partial K} := \int_{\partial K} q\,p.$$

The same notation is used on $\mathcal{T}_h^d$ and $\partial\mathcal{T}_h^d$, and $\|\cdot\|_{\mathcal{T}_h}$, $\|\cdot\|_{\partial\mathcal{T}_h}$, etc., denote the induced norms. Note that in $\langle\cdot,\cdot\rangle_{\partial\mathcal{T}_h}$ each interior face is counted twice. All differential operators applied to discrete functions are understood elementwise.

As usual, for a given set $R$ such that $|R|>0$, we denote by $\mathbb{P}_k(R)$ the space of polynomials of degree at most $k\geq 0$ on $R$. We now proceed to define the HDG spaces for this analysis:

$$\begin{aligned}
\mathcal{P}_h &:= \{\phi_h \in L^2(\mathcal{T}_h^d) :\ \phi_h|_K \in \mathbb{P}_k(K) \quad \forall K\in\mathcal{T}_h^d\},\\
\mathcal{V}_h &:= \{\boldsymbol{v}_h \in [L^2(\mathcal{T}_h)]^3 :\ \boldsymbol{v}_h|_K \in [\mathbb{P}_k(K)]^3 \quad \forall K\in\mathcal{T}_h\},\\
\mathcal{M}_h^t &:= \{\boldsymbol{\beta} \in [L^2(\mathcal{E}_h)]^3 :\ \boldsymbol{\beta}|_F \in [\mathbb{P}_k(F)]^3,\ (\boldsymbol{\beta}\cdot\boldsymbol{n})|_F = 0 \quad \forall F\in\mathcal{E}_h\},\\
\mathcal{M}_h^t(0) &:= \{\boldsymbol{\beta} \in \mathcal{M}_h^t :\ \boldsymbol{\beta}|_F = \boldsymbol{0} \quad \forall F\in\mathcal{E}_h^\Gamma\},\\
\Lambda_h &:= \{\eta \in L^2(\mathcal{E}_h^d) :\ \eta|_F \in \mathbb{P}_k(F)\ \ \forall F\in\mathcal{E}_h^d,\\
&\qquad \eta|_F = 0\ \ \forall F\in\mathcal{E}_h^\Gamma,\quad \eta|_{\Gamma_0}\in\mathbb{R}\}.
\end{aligned} \tag{6}$$

The space $\Lambda_h$ is a discrete counterpart of the trace space of $\Theta$: its elements vanish on $\Gamma$ and take a single (unknown) constant value on the whole interface $\Gamma_0$. Functions in $\mathcal{M}_h^t$ and $\Lambda_h$ are single valued on each face. In the sequel, we present the fully discrete formulation: we use the backward Euler method in time and the previously defined spaces in the spatial variable.

### 3.2 Fully discrete HDG formulation

Let $0=t_0<t_1<\cdots<t_M=T$ be a uniform partition of the time interval $[0,T]$ with time step $\Delta t = t_m - t_{m-1}$, and define $\overline{\partial}_t\chi^m := (\Delta t)^{-1}(\chi^m-\chi^{m-1})$ to be the first-order discrete time derivative, where $\chi^m=\chi(t_m)$. Let $\Pi_V : [L^2(\Omega)]^3 \longrightarrow \mathcal{V}_h$ be the $L^2$-orthogonal projection onto $\mathcal{V}_h$. Then the fully discrete method reads: Given $\boldsymbol{u}_h^0 = \Pi_V\boldsymbol{u}_0$ (any extension of $\boldsymbol{u}_0$ to $\Omega$ may be used, since only $\sigma\boldsymbol{u}_h^0$ enters the scheme), find, for each $1\leq m\leq M$,

$$(\boldsymbol{z}_h^m, \boldsymbol{u}_h^m, \varphi_h^m, \widehat{\boldsymbol{u}}_h^{t,m}, \widehat{\varphi}_h^m) \in \mathcal{V}_h\times\mathcal{V}_h\times\mathcal{P}_h\times\mathcal{M}_h^t\times\Lambda_h$$

such that

$$\begin{aligned}
(\mu\boldsymbol{z}_h^m, \boldsymbol{w})_{\mathcal{T}_h} - (\boldsymbol{u}_h^m, \mathbf{curl}\,\boldsymbol{w})_{\mathcal{T}_h} - \langle\widehat{\boldsymbol{u}}_h^{t,m}, \boldsymbol{w}\times\boldsymbol{n}\rangle_{\partial\mathcal{T}_h} &= 0,\\
(\sigma\overline{\partial}_t\boldsymbol{u}_h^m, \boldsymbol{v})_{\mathcal{T}_h} + (\boldsymbol{z}_h^m, \mathbf{curl}\,\boldsymbol{v})_{\mathcal{T}_h} + \langle\widehat{\boldsymbol{z}}_h^{t,m}, \boldsymbol{v}\times\boldsymbol{n}\rangle_{\partial\mathcal{T}_h}&\\
+ (\varphi_h^m, \mathrm{div}(\varepsilon\boldsymbol{v}))_{\mathcal{T}_h^d} - \langle\varepsilon\boldsymbol{v}\cdot\boldsymbol{n}, \widehat{\varphi}_h^m\rangle_{\partial\mathcal{T}_h^d} &= -(\overline{\partial}_t\mathbf{J}^m, \boldsymbol{v})_{\mathcal{T}_h},\\
(\varphi_h^m, \psi)_{\mathcal{T}_h^d} + (\varepsilon\boldsymbol{u}_h^m, \nabla\psi)_{\mathcal{T}_h^d} - \langle\varepsilon\widehat{\boldsymbol{u}}_h^{n,m}\cdot\boldsymbol{n}, \psi\rangle_{\partial\mathcal{T}_h^d} &= 0,\\
\langle\boldsymbol{n}\times\widehat{\boldsymbol{z}}_h^{t,m}, \boldsymbol{\beta}\rangle_{\partial\mathcal{T}_h\setminus\Gamma} &= 0,\\
\langle\varepsilon\widehat{\boldsymbol{u}}_h^{n,m}\cdot\boldsymbol{n}, \eta\rangle_{\partial\mathcal{T}_h^d} &= 0,\\
\langle\boldsymbol{n}\times\widehat{\boldsymbol{u}}_h^{t,m}, \boldsymbol{\beta}\rangle_{\Gamma} &= \langle\boldsymbol{g}^m, \boldsymbol{\beta}\rangle_{\Gamma},
\end{aligned} \tag{7}$$

for all

$$(\boldsymbol{w}, \boldsymbol{v}, \psi, \boldsymbol{\beta}, \eta) \in \mathcal{V}_h \times \mathcal{V}_h \times \mathcal{P}_h \times \mathcal{M}_h^t \times \Lambda_h.$$

The tangential and normal numerical fluxes, $\widehat{\boldsymbol{z}}_h^{t,m}$ and $\widehat{\boldsymbol{u}}_h^{n,m}$ respectively, at time level $t_m$, are defined by

$$\begin{aligned} \boldsymbol{n} \times \widehat{\boldsymbol{z}}_h^{t,m} &= \boldsymbol{n} \times \boldsymbol{z}_h^m + \tau_t(\boldsymbol{u}_h^{t,m} - \widehat{\boldsymbol{u}}_h^{t,m}) \qquad \text{on } \partial\mathcal{T}_h, \\ \varepsilon\widehat{\boldsymbol{u}}_h^{n,m} \cdot \boldsymbol{n} &= \varepsilon\boldsymbol{u}_h^m \cdot \boldsymbol{n} - \tau_n(\varphi_h^m - \widehat{\varphi}_h^m) \qquad \text{on } \partial\mathcal{T}_h^d, \end{aligned} \tag{8}$$

where $\tau_t > 0$ and $\tau_n > 0$ are stabilization parameters, which for simplicity we take constant. We stress that $\widehat{\boldsymbol{z}}_h^{t,m}$ and $\widehat{\boldsymbol{u}}_h^{n,m}$ are not unknowns: they are given in terms of the unknowns by (8), whereas the numerical trace $\widehat{\varphi}_h^m \in \Lambda_h$ is an unknown of the scheme. The first three equations in (7) are the local problems; the fourth and fifth ones impose the weak continuity of the tangential and normal fluxes, and the last one imposes the boundary condition. Since the fourth equation only involves faces not lying on $\Gamma$ and the last one only faces on $\Gamma$, the number of equations equals the number of unknowns.

We also remark that, taking in the fifth equation of (7) the function $\eta \in \Lambda_h$ equal to 1 on $\Gamma_0$ and 0 elsewhere, we obtain

$$\sum_{F \in \mathcal{E}_h^{\Gamma_0}} \int_F \varepsilon\widehat{\boldsymbol{u}}_h^{n,m} \cdot \boldsymbol{n} = 0,$$

which is the discrete counterpart of $\langle \varepsilon\boldsymbol{u}|_{\Omega_\mathrm{d}} \cdot \boldsymbol{n}_0, 1\rangle_{\Gamma_0} = 0$. This condition is thus imposed without penalty parameters, and only adds one global scalar unknown (the value of $\widehat{\varphi}_h^m$ on $\Gamma_0$), so that the static condensation remains local.

We begin with an algebraic identity that will be used repeatedly in the sequel.

**Lemma 3** *Let $(\boldsymbol{z}_h, \boldsymbol{u}_h, \varphi_h, \widehat{\boldsymbol{u}}_h^t, \widehat{\varphi}_h) \in \mathcal{V}_h \times \mathcal{V}_h \times \mathcal{P}_h \times \mathcal{M}_h^t \times \Lambda_h$, and let $\boldsymbol{n} \times \widehat{\boldsymbol{z}}_h^t$ and $\varepsilon\widehat{\boldsymbol{u}}_h^n \cdot \boldsymbol{n}$ be given by* (8) *(without the superscript $m$). Then*

$$\begin{aligned} &(\mu\boldsymbol{z}_h, \boldsymbol{z}_h)_{\mathcal{T}_h} - (\boldsymbol{u}_h, \mathbf{curl}\,\boldsymbol{z}_h)_{\mathcal{T}_h} - \langle \widehat{\boldsymbol{u}}_h^t, \boldsymbol{z}_h \times \boldsymbol{n}\rangle_{\partial\mathcal{T}_h} \\ &\quad + (\boldsymbol{z}_h, \mathbf{curl}\,\boldsymbol{u}_h)_{\mathcal{T}_h} + \langle \widehat{\boldsymbol{z}}_h^t, \boldsymbol{u}_h \times \boldsymbol{n}\rangle_{\partial\mathcal{T}_h} \\ &\quad + (\varphi_h, \mathrm{div}(\varepsilon\boldsymbol{u}_h))_{\mathcal{T}_h^d} - \langle \varepsilon\boldsymbol{u}_h \cdot \boldsymbol{n}, \widehat{\varphi}_h\rangle_{\partial\mathcal{T}_h^d} \\ &\quad + (\varphi_h, \varphi_h)_{\mathcal{T}_h^d} + (\varepsilon\boldsymbol{u}_h, \nabla\varphi_h)_{\mathcal{T}_h^d} - \langle \varepsilon\widehat{\boldsymbol{u}}_h^n \cdot \boldsymbol{n}, \varphi_h\rangle_{\partial\mathcal{T}_h^d} \\ &\quad - \langle \boldsymbol{n} \times \widehat{\boldsymbol{z}}_h^t, \widehat{\boldsymbol{u}}_h^t\rangle_{\partial\mathcal{T}_h} + \langle \varepsilon\widehat{\boldsymbol{u}}_h^n \cdot \boldsymbol{n}, \widehat{\varphi}_h\rangle_{\partial\mathcal{T}_h^d} \\ &= \|\sqrt{\mu}\,\boldsymbol{z}_h\|_{\mathcal{T}_h}^2 + \|\varphi_h\|_{\mathcal{T}_h^d}^2 \\ &\quad + \tau_t \left\|\boldsymbol{u}_h^t - \widehat{\boldsymbol{u}}_h^t\right\|_{\partial\mathcal{T}_h}^2 + \tau_n \left\|\varphi_h - \widehat{\varphi}_h\right\|_{\partial\mathcal{T}_h^d}^2. \end{aligned} \tag{9}$$

**Proof.** We employ the elementwise integration-by-parts identities

$$(\boldsymbol{z}_h, \mathbf{curl}\,\boldsymbol{u}_h)_{\mathcal{T}_h} - (\boldsymbol{u}_h, \mathbf{curl}\,\boldsymbol{z}_h)_{\mathcal{T}_h} = \langle \boldsymbol{n} \times \boldsymbol{u}_h, \boldsymbol{z}_h\rangle_{\partial\mathcal{T}_h},$$

and

$$(\varphi_h, \mathrm{div}(\varepsilon\boldsymbol{u}_h))_{\mathcal{T}_h^d} + (\varepsilon\boldsymbol{u}_h, \nabla\varphi_h)_{\mathcal{T}_h^d} = \langle \varepsilon\boldsymbol{u}_h \cdot \boldsymbol{n}, \varphi_h\rangle_{\partial\mathcal{T}_h^d},$$

together with $\langle \widehat{\boldsymbol{u}}_h^t, \boldsymbol{z}_h \times \boldsymbol{n}\rangle_{\partial\mathcal{T}_h} = \langle \boldsymbol{n}\times\widehat{\boldsymbol{u}}_h^t, \boldsymbol{z}_h\rangle_{\partial\mathcal{T}_h}$, $\langle \widehat{\boldsymbol{z}}_h^t, \boldsymbol{u}_h \times \boldsymbol{n}\rangle_{\partial\mathcal{T}_h} = \langle \boldsymbol{n}\times\widehat{\boldsymbol{z}}_h^t, \boldsymbol{u}_h\rangle_{\partial\mathcal{T}_h}$, and $(\boldsymbol{n}\times\mathbf{a})\cdot\mathbf{b} = -(\boldsymbol{n}\times\mathbf{b})\cdot\mathbf{a}$. Then, the terms involving $\boldsymbol{z}_h$ and $\boldsymbol{u}_h$ in (9) reduce to

$$\|\sqrt{\mu}\,\boldsymbol{z}_h\|_{\mathcal{T}_h}^2 + \langle \boldsymbol{n}\times(\widehat{\boldsymbol{z}}_h^t - \boldsymbol{z}_h), \boldsymbol{u}_h - \widehat{\boldsymbol{u}}_h^t\rangle_{\partial\mathcal{T}_h} = \|\sqrt{\mu}\,\boldsymbol{z}_h\|_{\mathcal{T}_h}^2 + \tau_t \left\|\boldsymbol{u}_h^t - \widehat{\boldsymbol{u}}_h^t\right\|_{\partial\mathcal{T}_h}^2,$$

where we used (8) and the fact that, $\widehat{\boldsymbol{u}}_h^t$ being tangential, $(\boldsymbol{u}_h^t - \widehat{\boldsymbol{u}}_h^t)\cdot(\boldsymbol{u}_h - \widehat{\boldsymbol{u}}_h^t) = |\boldsymbol{u}_h^t - \widehat{\boldsymbol{u}}_h^t|^2$. Similarly, the terms involving $\varphi_h$ reduce to

$$\|\varphi_h\|_{\mathcal{T}_h^d}^2 + \langle \varepsilon(\boldsymbol{u}_h\cdot\boldsymbol{n} - \widehat{\boldsymbol{u}}_h^n\cdot\boldsymbol{n}), \varphi_h - \widehat{\varphi}_h\rangle_{\partial\mathcal{T}_h^d} = \|\varphi_h\|_{\mathcal{T}_h^d}^2 + \tau_n\,\|\varphi_h - \widehat{\varphi}_h\|_{\partial\mathcal{T}_h^d}^2,$$

by virtue of (8). □

**Theorem 4 (Existence and uniqueness of the fully discrete HDG problem)** *For each $1 \le m \le M$, the fully discrete HDG problem* (7)–(8) *admits a unique solution*

$$(\boldsymbol{z}_h^m, \boldsymbol{u}_h^m, \varphi_h^m, \widehat{\boldsymbol{u}}_h^{t,m}, \widehat{\varphi}_h^m) \in \mathcal{V}_h \times \mathcal{V}_h \times \mathcal{P}_h \times \mathcal{M}_h^t \times \Lambda_h.$$

**Proof.** Since the scheme is linear and all discrete spaces are finite dimensional, it suffices to prove uniqueness, that is, that the homogeneous problem (7)–(8) with

$$\bar{\partial}_t \mathbf{J}^m = \mathbf{0}, \qquad \boldsymbol{g}^m = \mathbf{0}, \qquad \boldsymbol{u}_h^{m-1} = \mathbf{0}\,,$$

only has the trivial solution. Let $(\boldsymbol{z}_h^m, \boldsymbol{u}_h^m, \varphi_h^m, \widehat{\boldsymbol{u}}_h^{t,m}, \widehat{\varphi}_h^m)$ be a solution of this homogeneous problem. From the last equation of (7), $\widehat{\boldsymbol{u}}_h^{t,m} = \mathbf{0}$ on $\Gamma$, that is, $\widehat{\boldsymbol{u}}_h^{t,m} \in \mathcal{M}_h^t(0)$. Testing the homogeneous system with

$$\boldsymbol{w} = \boldsymbol{z}_h^m, \qquad \boldsymbol{v} = \boldsymbol{u}_h^m, \qquad \psi = \varphi_h^m, \qquad \boldsymbol{\beta} = -\widehat{\boldsymbol{u}}_h^{t,m}, \qquad \eta = \widehat{\varphi}_h^m,$$

adding the resulting equations, and applying Lemma 3, we obtain the identity

$$\begin{aligned}(\Delta t)^{-1}\left\|\sqrt{\sigma}\,\boldsymbol{u}_h^m\right\|_{\mathcal{T}_h}^2 + \|\sqrt{\mu}\,\boldsymbol{z}_h^m\|_{\mathcal{T}_h}^2 + \|\varphi_h^m\|_{\mathcal{T}_h^d}^2 \\ + \tau_t\|\boldsymbol{u}_h^{t,m} - \widehat{\boldsymbol{u}}_h^{t,m}\|_{\partial\mathcal{T}_h}^2 + \tau_n\|\varphi_h^m - \widehat{\varphi}_h^m\|_{\partial\mathcal{T}_h^d}^2 = 0.\end{aligned} \tag{10}$$

Consequently, $\boldsymbol{z}_h^m = \mathbf{0}$ in $\Omega$, $\varphi_h^m = 0$ in $\Omega_{\mathtt{d}}$, $\boldsymbol{u}_h^m = \mathbf{0}$ in $\Omega_{\mathtt{c}}$, $\widehat{\boldsymbol{u}}_h^{t,m} = \boldsymbol{u}_h^{t,m}$ on $\partial\mathcal{T}_h$, and $\widehat{\varphi}_h^m = 0$ on $\partial\mathcal{T}_h^d$. It remains to show that $\boldsymbol{u}_h^m = \mathbf{0}$ in $\Omega_{\mathtt{d}}$, which we do in four steps.

*Step 1.* Since $\boldsymbol{z}_h^m = \mathbf{0}$ and $\widehat{\boldsymbol{u}}_h^{t,m} = \boldsymbol{u}_h^{t,m}$, the first equation of (7) and an elementwise integration by parts give $(\mathbf{curl}\,\boldsymbol{u}_h^m, \boldsymbol{w})_{\mathcal{T}_h} = 0$ for all $\boldsymbol{w} \in \mathcal{V}_h$, whence $\mathbf{curl}\,\boldsymbol{u}_h^m|_K = \mathbf{0}$ for all $K \in \mathcal{T}_h$. Moreover, $\boldsymbol{u}_h^{t,m} = \widehat{\boldsymbol{u}}_h^{t,m}$ is single valued on interior faces and vanishes on $\Gamma$. Hence $\boldsymbol{u}_h^m \in \mathbf{H}_0(\mathbf{curl};\Omega)$ and $\mathbf{curl}\,\boldsymbol{u}_h^m = \mathbf{0}$. Since $\Omega$ is simply connected and $\Gamma$ is connected, there exists $p \in H_0^1(\Omega)$ such that $\boldsymbol{u}_h^m = \nabla p$ (see, e.g., [9]).

*Step 2.* Since $\nabla p = \boldsymbol{u}_h^m = \mathbf{0}$ in $\Omega_{\mathtt{c}}$ and $\Omega_{\mathtt{c}}$ is connected, $p = c_0$ in $\Omega_{\mathtt{c}}$ for some $c_0 \in \mathbb{R}$, and hence $p|_{\Gamma_0} = c_0$.

*Step 3.* Since $\varphi_h^m = \widehat{\varphi}_h^m = 0$, (8) gives $\varepsilon\widehat{\boldsymbol{u}}_h^{n,m}\cdot\boldsymbol{n} = \varepsilon\boldsymbol{u}_h^m\cdot\boldsymbol{n}$. Then, the third equation of (7) yields $(\mathrm{div}(\varepsilon\boldsymbol{u}_h^m), \psi)_K = 0$ for all $\psi \in \mathbb{P}_k(K)$ and, $\varepsilon$ being constant on $K$, $\mathrm{div}(\varepsilon\boldsymbol{u}_h^m)|_K = 0$ for all $K \in \mathcal{T}_h^d$. Taking in the fifth equation of (7) $\eta$ supported on a single interior face $F \in \mathcal{E}_h^d$, and noting that the jump of $\varepsilon\boldsymbol{u}_h^m\cdot\boldsymbol{n}$ across $F$ belongs to $\mathbb{P}_k(F)$, we deduce that this jump vanishes. Therefore $\varepsilon\boldsymbol{u}_h^m|_{\Omega_{\mathtt{d}}} \in \mathbf{H}(\mathrm{div};\Omega_{\mathtt{d}})$ with $\mathrm{div}(\varepsilon\boldsymbol{u}_h^m) = 0$ in $\Omega_{\mathtt{d}}$. Finally, taking $\eta = 1$ on $\Gamma_0$ and 0 elsewhere, $\langle \varepsilon\boldsymbol{u}_h^m\cdot\boldsymbol{n}_0, 1\rangle_{\Gamma_0} = 0$.

*Step 4.* Integrating by parts in $\Omega_{\mathtt{d}}$, and using Steps 2 and 3 and $p = 0$ on $\Gamma$,

$$(\varepsilon \boldsymbol{u}_h^m, \boldsymbol{u}_h^m)_{\Omega_{\mathtt{d}}} = (\varepsilon \boldsymbol{u}_h^m, \nabla p)_{\Omega_{\mathtt{d}}} = -(\mathrm{div}(\varepsilon \boldsymbol{u}_h^m), p)_{\Omega_{\mathtt{d}}} + c_0 \, \langle \varepsilon \boldsymbol{u}_h^m \cdot \boldsymbol{n}_0, 1 \rangle_{\Gamma_0} = 0.$$

Hence $\boldsymbol{u}_h^m = \mathbf{0}$ in $\Omega_{\mathtt{d}}$, and then $\widehat{\boldsymbol{u}}_h^{t,m} = \boldsymbol{u}_h^{t,m} = \mathbf{0}$. Therefore, the homogeneous problem has only the trivial solution. This proves uniqueness. Existence now follows from linearity of the scheme and the finite dimensionality of the discrete spaces. □

In contrast to stationary HDG formulations for Maxwell-type problems, where stability and well-posedness can be established through coercivity arguments and energy identities associated with the numerical fluxes (see, e.g., [16]), the analysis of time-dependent problems requires an additional discrete energy estimate. Indeed, the presence of the time derivative introduces an evolution mechanism that cannot be controlled solely by the spatial stability of the method. A discrete energy argument is therefore essential to guarantee stability with respect to time, to prevent the growth of numerical errors, and to derive a priori error estimates for the fully discrete scheme. An additional difficulty here is that $\sigma$ vanishes in $\Omega_{\mathtt{d}}$, so that the time derivative only provides control of the electric field in the conductor. In particular, the source term cannot be bounded by a direct duality argument against $\boldsymbol{u}_h^m$ in $\Omega_{\mathtt{d}}$. Instead, we use the following discrete integration-by-parts formula, which transfers the curl of the source onto $\boldsymbol{z}_h^m$ and onto the stabilization term.

**Lemma 5** *Let $\mathbf{a} \in [H^1(\Omega)]^3$, and let $(\boldsymbol{p}_h, \boldsymbol{v}_h, \boldsymbol{\beta}_h) \in \mathcal{V}_h \times \mathcal{V}_h \times \mathcal{M}_h^t(0)$ satisfy*

$$(\mu \boldsymbol{p}_h, \boldsymbol{w})_{\mathcal{T}_h} - (\boldsymbol{v}_h, \mathbf{curl}\, \boldsymbol{w})_{\mathcal{T}_h} - \langle \boldsymbol{\beta}_h, \boldsymbol{w} \times \boldsymbol{n} \rangle_{\partial \mathcal{T}_h} = 0 \qquad \forall\, \boldsymbol{w} \in \mathcal{V}_h. \tag{11}$$

*Then*

$$(\mathbf{curl}\, \mathbf{a}, \boldsymbol{v}_h)_{\mathcal{T}_h} = (\mu \boldsymbol{p}_h, \Pi_V \mathbf{a})_{\mathcal{T}_h} + \langle \boldsymbol{n} \times (\mathbf{a} - \Pi_V \mathbf{a}), \boldsymbol{v}_h^t - \boldsymbol{\beta}_h \rangle_{\partial \mathcal{T}_h}. \tag{12}$$

*Consequently, there exists $C > 0$, independent of $h$, such that*

$$|(\mathbf{curl}\, \mathbf{a}, \boldsymbol{v}_h)_{\mathcal{T}_h}| \le \overline{\mu}^{1/2} \, \|\sqrt{\mu}\, \boldsymbol{p}_h\|_{\mathcal{T}_h} \, \|\mathbf{a}\|_{\mathcal{T}_h} + C\, h^{1/2} |\mathbf{a}|_{H^1(\Omega)} \left\| \boldsymbol{v}_h^t - \boldsymbol{\beta}_h \right\|_{\partial \mathcal{T}_h}. \tag{13}$$

**Proof.** Integrating by parts elementwise, we have

$$(\mathbf{curl}\, \mathbf{a}, \boldsymbol{v}_h)_{\mathcal{T}_h} = (\mathbf{a}, \mathbf{curl}\, \boldsymbol{v}_h)_{\mathcal{T}_h} + \langle \boldsymbol{n} \times \mathbf{a}, \boldsymbol{v}_h \rangle_{\partial \mathcal{T}_h}.$$

Since $\mathbf{a} \in [H^1(\Omega)]^3$, its tangential trace is single valued and, since $\boldsymbol{\beta}_h$ is single valued and vanishes on $\Gamma$, we get $\langle \boldsymbol{n} \times \mathbf{a}, \boldsymbol{\beta}_h \rangle_{\partial \mathcal{T}_h} = 0$. In addition, $\mathbf{curl}\, \boldsymbol{v}_h \in \mathcal{V}_h$, so that $(\mathbf{a}, \mathbf{curl}\, \boldsymbol{v}_h)_{\mathcal{T}_h} = (\Pi_V \mathbf{a}, \mathbf{curl}\, \boldsymbol{v}_h)_{\mathcal{T}_h}$. Integrating by parts back and using (11) with $\boldsymbol{w} = \Pi_V \mathbf{a}$, we find

$$\begin{aligned} (\Pi_V \mathbf{a}, \mathbf{curl}\, \boldsymbol{v}_h)_{\mathcal{T}_h} &= (\boldsymbol{v}_h, \mathbf{curl}\, \Pi_V \mathbf{a})_{\mathcal{T}_h} + \langle \boldsymbol{n} \times \boldsymbol{v}_h, \Pi_V \mathbf{a} \rangle_{\partial \mathcal{T}_h} \\ &= (\mu \boldsymbol{p}_h, \Pi_V \mathbf{a})_{\mathcal{T}_h} - \langle \boldsymbol{n} \times \Pi_V \mathbf{a}, \boldsymbol{v}_h - \boldsymbol{\beta}_h \rangle_{\partial \mathcal{T}_h}. \end{aligned}$$

Collecting terms, and noting that $\boldsymbol{n} \times (\cdot)$ is tangential, we obtain (12). The bound (13) follows from the Cauchy–Schwarz inequality, $\|\Pi_V \mathbf{a}\|_{\mathcal{T}_h} \le \|\mathbf{a}\|_{\mathcal{T}_h}$, and the estimate $\|\mathbf{a} - \Pi_V \mathbf{a}\|_{\partial K} \le C h_K^{1/2} |\mathbf{a}|_{H^1(K)}$ (see Lemma 8 below). □

**Theorem 6 (Discrete energy stability)** *Assume $\boldsymbol{g} = \mathbf{0}$, and let $(\boldsymbol{z}_h^m, \boldsymbol{u}_h^m, \varphi_h^m, \widehat{\boldsymbol{u}}_h^{t,m}, \widehat{\varphi}_h^m)$ be the solution of the fully discrete problem (7)–(8) at time level $t_m$. Then there exists a constant $C > 0$ independent of $h$ and $\Delta t$ such that, for each $\ell \in \{1, \ldots, M\}$, there holds*

$$\begin{aligned}
&\Big\|\sqrt{\sigma}\,\boldsymbol{u}_h^\ell\Big\|_{\mathcal{T}_h}^2 + \Delta t \sum_{m=1}^{\ell} \Big( \|\sqrt{\mu}\,\boldsymbol{z}_h^m\|_{\mathcal{T}_h}^2 + 2\|\varphi_h^m\|_{\mathcal{T}_h^d}^2 \\
&\qquad + \tau_t \|\boldsymbol{u}_h^{t,m} - \widehat{\boldsymbol{u}}_h^{t,m}\|_{\partial\mathcal{T}_h}^2 + 2\tau_n \|\varphi_h^m - \widehat{\varphi}_h^m\|_{\partial\mathcal{T}_h^d}^2 \Big) \\
&\leq \big\|\sqrt{\sigma}\,\boldsymbol{u}_h^0\big\|_{\mathcal{T}_h}^2 \\
&\qquad + \big(\overline{\mu} + C\,h\,\tau_t^{-1}\big)\,\|\partial_t \mathbf{H}_{\mathbf{s}}\|_{L^2(0,T;[H^1(\Omega)]^3)}^2.
\end{aligned} \tag{14}$$

**Proof.** First, we fix $m \in \{1, \ldots, M\}$. Since $\boldsymbol{g} = \mathbf{0}$, we have $\widehat{\boldsymbol{u}}_h^{t,m} \in \mathcal{M}_h^t(0)$. In a similar way to Theorem 4, we take as test functions in (7)

$$\boldsymbol{w} = \boldsymbol{z}_h^m, \qquad \boldsymbol{v} = \boldsymbol{u}_h^m, \qquad \psi = \varphi_h^m, \qquad \boldsymbol{\beta} = -\widehat{\boldsymbol{u}}_h^{t,m}, \qquad \eta = \widehat{\varphi}_h^m.$$

Adding the resulting equations and applying Lemma 3, we obtain:

$$\begin{aligned}
&(\sigma\overline{\partial}_t \boldsymbol{u}_h^m, \boldsymbol{u}_h^m)_{\mathcal{T}_h} + \|\sqrt{\mu}\,\boldsymbol{z}_h^m\|_{\mathcal{T}_h}^2 + \|\varphi_h^m\|_{\mathcal{T}_h^d}^2 \\
&\qquad + \tau_t \|\boldsymbol{u}_h^{t,m} - \widehat{\boldsymbol{u}}_h^{t,m}\|_{\partial\mathcal{T}_h}^2 + \tau_n \|\varphi_h^m - \widehat{\varphi}_h^m\|_{\partial\mathcal{T}_h^d}^2 \\
&\qquad = -(\mathbf{curl}\,\overline{\partial}_t \mathbf{H}_{\mathbf{s}}^m, \boldsymbol{u}_h^m)_{\mathcal{T}_h}.
\end{aligned} \tag{15}$$

For the temporal term, we employ the identity $2(a-b)a = a^2 - b^2 + (a-b)^2$. Thus, we have:

$$\begin{aligned}
(\sigma\overline{\partial}_t \boldsymbol{u}_h^m, \boldsymbol{u}_h^m)_{\mathcal{T}_h} &= \frac{1}{2\Delta t}\Big[\big\|\sqrt{\sigma}\,\boldsymbol{u}_h^m\big\|_{\mathcal{T}_h}^2 - \big\|\sqrt{\sigma}\,\boldsymbol{u}_h^{m-1}\big\|_{\mathcal{T}_h}^2 \\
&\qquad + \big\|\sqrt{\sigma}\,(\boldsymbol{u}_h^m - \boldsymbol{u}_h^{m-1})\big\|_{\mathcal{T}_h}^2\Big] \\
&\geq \frac{1}{2\Delta t}\Big[\big\|\sqrt{\sigma}\,\boldsymbol{u}_h^m\big\|_{\mathcal{T}_h}^2 - \big\|\sqrt{\sigma}\,\boldsymbol{u}_h^{m-1}\big\|_{\mathcal{T}_h}^2\Big].
\end{aligned} \tag{16}$$

Now we estimate the right-hand side term of (15). Invoking Lemma 5, with $\mathbf{a} = \overline{\partial}_t \mathbf{H}_{\mathbf{s}}^m$ and $(\boldsymbol{p}_h, \boldsymbol{v}_h, \boldsymbol{\beta}_h) = (\boldsymbol{z}_h^m, \boldsymbol{u}_h^m, \widehat{\boldsymbol{u}}_h^{t,m})$, and after applying Young's inequality, we deduce

$$\begin{aligned}
|(\mathbf{curl}\,\overline{\partial}_t \mathbf{H}_{\mathbf{s}}^m, \boldsymbol{u}_h^m)_{\mathcal{T}_h}| &\leq \frac{1}{2}\,\|\sqrt{\mu}\,\boldsymbol{z}_h^m\|_{\mathcal{T}_h}^2 + \frac{\overline{\mu}}{2}\|\overline{\partial}_t \mathbf{H}_{\mathbf{s}}^m\|_{\mathcal{T}_h}^2 \\
&\qquad + \frac{\tau_t}{2}\|\boldsymbol{u}_h^{t,m} - \widehat{\boldsymbol{u}}_h^{t,m}\|_{\partial\mathcal{T}_h}^2 + \frac{C\,h}{2\tau_t}|\overline{\partial}_t \mathbf{H}_{\mathbf{s}}^m|_{H^1(\Omega)}^2.
\end{aligned} \tag{17}$$

Substituting (16) and (17) into (15), and multiplying by $2\Delta t$, we obtain:

$$\begin{aligned}
&\big\|\sqrt{\sigma}\,\boldsymbol{u}_h^m\big\|_{\mathcal{T}_h}^2 - \big\|\sqrt{\sigma}\,\boldsymbol{u}_h^{m-1}\big\|_{\mathcal{T}_h}^2 + \Delta t\Big( \|\sqrt{\mu}\,\boldsymbol{z}_h^m\|_{\mathcal{T}_h}^2 + 2\|\varphi_h^m\|_{\mathcal{T}_h^d}^2 \\
&\quad + \tau_t \|\boldsymbol{u}_h^{t,m} - \widehat{\boldsymbol{u}}_h^{t,m}\|_{\partial\mathcal{T}_h}^2 + 2\tau_n \|\varphi_h^m - \widehat{\varphi}_h^m\|_{\partial\mathcal{T}_h^d}^2 \Big) \\
&\quad \leq \Delta t\,\big(\overline{\mu} + C\,h\,\tau_t^{-1}\big)\|\overline{\partial}_t \mathbf{H}_{\mathbf{s}}^m\|_{H^1(\Omega)}^2.
\end{aligned} \tag{18}$$

At this point we notice that $\overline{\partial}_t \mathbf{H}_{\mathbf{s}}^m = (\Delta t)^{-1} \int_{t_{m-1}}^{t_m} \partial_t \mathbf{H}_{\mathbf{s}}\, ds$. Cauchy–Schwarz inequality gives

$$\Delta t \sum_{m=1}^{\ell} \|\overline{\partial}_t \mathbf{H}_{\mathbf{s}}^m\|_{H^1(\Omega)}^2 \leq \|\partial_t \mathbf{H}_{\mathbf{s}}\|_{L^2(0,T;[H^1(\Omega)]^3)}^2 . \tag{19}$$

Then, summing up (18) from $m = 1$ to $m = \ell \in \{1, ..., M\}$, and after applying telescopic property and (19), we arrive to (14) and we end the proof. □

**Remark 7** *Thanks to the telescoping structure of the $\sigma$-weighted norm, no discrete Gronwall argument is needed in the proof of Theorem 6; hence the scheme is unconditionally stable and the constant in* (14) *does not depend on $T$. Note also that $\left\|\sqrt{\sigma}\, \boldsymbol{u}_h^0\right\|_{\mathcal{T}_h} \leq \overline{\sigma}^{1/2} \|\boldsymbol{u}_0\|_{\Omega_c}$.*

# 4 Error estimates

In this section, we conduct the a priori error analysis of the HDG method. For this purpose, we begin by introducing the projectors, followed by the derivation of the error equation. We conclude by establishing the convergence properties of the method.

## 4.1 $L^2$-orthogonal projections and their approximation properties

We use the $L^2$-orthogonal projection $\Pi_V : [L^2(\Omega)]^3 \to \mathcal{V}_h$ introduced above, both for $\boldsymbol{z}$ and $\boldsymbol{u}$; to keep the notation, we write $\Pi_W := \Pi_V$ when it is applied to $\boldsymbol{z}$. For the tangential traces, we introduce the space $L_t^2(\mathcal{E}_h) := \{\boldsymbol{\beta} \in [L^2(\mathcal{E}_h)]^3 : \ (\boldsymbol{\beta} \cdot \boldsymbol{n})|_F = 0 \ \forall F \in \mathcal{E}_h\}$ and the facewise $L^2$-orthogonal projection $\Pi_M^t : L_t^2(\mathcal{E}_h) \to \mathcal{M}_h^t$, defined by

$$\langle \Pi_M^t \boldsymbol{\beta} - \boldsymbol{\beta}, \boldsymbol{\gamma} \rangle_F = 0 \qquad \forall\, \boldsymbol{\gamma} \in \mathcal{M}_h^t|_F, \quad \forall F \in \mathcal{E}_h. \tag{20}$$

Since the exact multiplier vanishes (cf. Proposition 2), no projection is needed for $\varphi$ and its trace.

**Lemma 8** *The projections $\Pi_V$ and $\Pi_M^t$ satisfy the following properties:*

*(i) For $\kappa \in \{\mu, \sigma, \varepsilon\}$ and every $\boldsymbol{w} \in [L^2(\Omega)]^3$, $(\kappa(\boldsymbol{w} - \Pi_V \boldsymbol{w}), \boldsymbol{v})_{\mathcal{T}_h} = 0$ for all $\boldsymbol{v} \in \mathcal{V}_h$. In particular, $(\boldsymbol{w} - \Pi_V \boldsymbol{w}, \mathbf{curl}\, \boldsymbol{v})_{\mathcal{T}_h} = 0$ for all $\boldsymbol{v} \in \mathcal{V}_h$, and $(\varepsilon(\boldsymbol{w} - \Pi_V \boldsymbol{w}), \nabla \psi)_{\mathcal{T}_h^d} = 0$ for all $\psi \in \mathcal{P}_h$.*

*(ii) $\Pi_V$ commutes with $\overline{\partial}_t$, that is, $\overline{\partial}_t \Pi_V \boldsymbol{w}^m = \Pi_V \overline{\partial}_t \boldsymbol{w}^m$.*

*(iii) For every $\boldsymbol{\beta} \in L_t^2(\mathcal{E}_h)$, $\boldsymbol{v} \in \mathcal{V}_h$ and $F \in \mathcal{E}_h$, there hold $\langle \boldsymbol{\beta} - \Pi_M^t \boldsymbol{\beta}, \boldsymbol{v} \rangle_F = \langle \boldsymbol{\beta} - \Pi_M^t \boldsymbol{\beta}, \boldsymbol{v} \times \boldsymbol{n} \rangle_F = 0$, since $\boldsymbol{v}^t|_F$ and $(\boldsymbol{v} \times \boldsymbol{n})|_F$ belong to $\mathcal{M}_h^t|_F$.*

*(iv) There exists a constant $C > 0$, independent of $h$, such that for all $K \in \mathcal{T}_h$, $\boldsymbol{w} \in [H^s(K)]^3$ and $1 \leq s \leq k+1$,*

$$\|\boldsymbol{w} - \Pi_V \boldsymbol{w}\|_K \leq C h_K^s |\boldsymbol{w}|_{H^s(K)}, \tag{21a}$$

$$\|\boldsymbol{w} - \Pi_V \boldsymbol{w}\|_{\partial K} \leq C h_K^{s-1/2} |\boldsymbol{w}|_{H^s(K)}. \tag{21b}$$

**Proof.** $(i)-(iii)$ follow directly from the definitions, since $\mu$, $\sigma$ and $\varepsilon$ are constant on each element, and $\kappa\boldsymbol{v}|_K$, $\mathbf{curl}\,\boldsymbol{v}|_K$ and $\nabla\psi|_K$ are polynomials of degree at most $k$. For the proof of $(iv)$we refer to [18, 22]. □

We also introduce the temporal consistency errors

$$\begin{aligned}&\widehat{\rho}_{\boldsymbol{u}}^m := \overline{\partial}_t\boldsymbol{u}^m - \partial_t\boldsymbol{u}(t_m), \qquad \boldsymbol{\xi}^m := \overline{\partial}_t\mathbf{H}_{\mathtt{s}}^m - \partial_t\mathbf{H}_{\mathtt{s}}(t_m),\\ &\text{so that}\quad \overline{\partial}_t\mathbf{J}^m - \partial_t\mathbf{J}(t_m) = \mathbf{curl}\,\boldsymbol{\xi}^m.\end{aligned} \tag{22}$$

Let $(\boldsymbol{z},\boldsymbol{u},\varphi) = (\boldsymbol{z},\boldsymbol{u},0)$ be the exact solution of (4), and assume that $\boldsymbol{z}(t),\boldsymbol{u}(t) \in [H^1(\mathcal{T}_h)]^3$. Since $\boldsymbol{z},\boldsymbol{u} \in \mathbf{H}(\mathbf{curl};\Omega)$ and $\varepsilon\boldsymbol{u}|_{\Omega_{\mathtt{d}}} \in \mathbf{H}(\mathrm{div};\Omega_{\mathtt{d}})$, the traces $\boldsymbol{u}^t$, $\boldsymbol{n}\times\boldsymbol{z}$ and $\varepsilon\boldsymbol{u}\cdot\boldsymbol{n}$ are single valued on interior faces (up to the orientation of $\boldsymbol{n}$). Then, it is readily seen that the HDG method is consistent: for each $m$, the quintuple $(\boldsymbol{z}(t_m),\boldsymbol{u}(t_m),0,\boldsymbol{u}^t(t_m),0)$ satisfies (7) (with numerical fluxes $\boldsymbol{n}\times\boldsymbol{z}(t_m)$ and $\varepsilon\boldsymbol{u}(t_m)\cdot\boldsymbol{n}$), with $\sigma\overline{\partial}_t\boldsymbol{u}_h^m$ and $\overline{\partial}_t\mathbf{J}^m$ replaced by $\sigma\partial_t\boldsymbol{u}(t_m)$ and $\partial_t\mathbf{J}(t_m)$, respectively. We decompose the errors into approximation and discrete components as follows:

$$\widehat{\delta}_{\boldsymbol{z}}^m := \boldsymbol{z}^m - \Pi_W\boldsymbol{z}^m, \qquad \widehat{\delta}_{\boldsymbol{u}}^m := \boldsymbol{u}^m - \Pi_V\boldsymbol{u}^m,$$

and

$$\boldsymbol{e}_{\boldsymbol{z}}^m := \Pi_W\boldsymbol{z}^m - \boldsymbol{z}_h^m, \qquad \boldsymbol{e}_{\boldsymbol{u}}^m := \Pi_V\boldsymbol{u}^m - \boldsymbol{u}_h^m, \qquad e_\varphi^m := -\varphi_h^m.$$

For the traces, we set

$$\boldsymbol{e}_{\widehat{\boldsymbol{u}}}^{t,m} := \Pi_M^t(\boldsymbol{u}^m)^t - \widehat{\boldsymbol{u}}_h^{t,m}, \qquad \widehat{e}_\varphi^m := -\widehat{\varphi}_h^m.$$

We also define the numerical flux errors by

$$\boldsymbol{n}\times\boldsymbol{e}_{\widehat{\boldsymbol{z}}}^{t,m} := \boldsymbol{n}\times\boldsymbol{e}_{\boldsymbol{z}}^m + \tau_t((\boldsymbol{e}_{\boldsymbol{u}}^m)^t - \boldsymbol{e}_{\widehat{\boldsymbol{u}}}^{t,m}), \tag{23}$$

and

$$\varepsilon\boldsymbol{e}_{\widehat{\boldsymbol{u}}}^{n,m}\cdot\boldsymbol{n} := \varepsilon\boldsymbol{e}_{\boldsymbol{u}}^m\cdot\boldsymbol{n} - \tau_n(e_\varphi^m - \widehat{e}_\varphi^m), \tag{24}$$

which have the same structure as (8).

Subtracting the fully discrete HDG scheme (7) from the consistency relations above, and inserting the projections, we obtain the following error system: for each $1 \le m \le M$,

$$(\mu\boldsymbol{e}_{\boldsymbol{z}}^m,\boldsymbol{w})_{\mathcal{T}_h} - (\boldsymbol{e}_{\boldsymbol{u}}^m,\mathbf{curl}\,\boldsymbol{w})_{\mathcal{T}_h} - \langle\boldsymbol{e}_{\widehat{\boldsymbol{u}}}^{t,m},\boldsymbol{w}\times\boldsymbol{n}\rangle_{\partial\mathcal{T}_h} = 0, \tag{25}$$

$$\begin{aligned}&(\sigma\overline{\partial}_t\boldsymbol{e}_{\boldsymbol{u}}^m,\boldsymbol{v})_{\mathcal{T}_h} + (\boldsymbol{e}_{\boldsymbol{z}}^m,\mathbf{curl}\,\boldsymbol{v})_{\mathcal{T}_h} + \langle\boldsymbol{n}\times\boldsymbol{e}_{\widehat{\boldsymbol{z}}}^{t,m},\boldsymbol{v}\rangle_{\partial\mathcal{T}_h}\\ &\quad + (e_\varphi^m,\mathrm{div}(\varepsilon\boldsymbol{v}))_{\mathcal{T}_h^d} - \langle\varepsilon\boldsymbol{v}\cdot\boldsymbol{n},\widehat{e}_\varphi^m\rangle_{\partial\mathcal{T}_h^d}\\ &\quad = (\sigma\widehat{\rho}_{\boldsymbol{u}}^m,\boldsymbol{v})_{\mathcal{T}_h} + (\mathbf{curl}\,\boldsymbol{\xi}^m,\boldsymbol{v})_{\mathcal{T}_h} - \langle\boldsymbol{n}\times\widehat{\delta}_{\boldsymbol{z}}^m + \tau_t(\widehat{\delta}_{\boldsymbol{u}}^m)^t,\boldsymbol{v}\rangle_{\partial\mathcal{T}_h},\end{aligned} \tag{26}$$

$$(e_\varphi^m,\psi)_{\mathcal{T}_h^d} + (\varepsilon\boldsymbol{e}_{\boldsymbol{u}}^m,\nabla\psi)_{\mathcal{T}_h^d} - \langle\varepsilon\boldsymbol{e}_{\widehat{\boldsymbol{u}}}^{n,m}\cdot\boldsymbol{n},\psi\rangle_{\partial\mathcal{T}_h^d} = \langle\varepsilon\widehat{\delta}_{\boldsymbol{u}}^m\cdot\boldsymbol{n},\psi\rangle_{\partial\mathcal{T}_h^d}, \tag{27}$$

$$\langle\boldsymbol{n}\times\boldsymbol{e}_{\widehat{\boldsymbol{z}}}^{t,m},\boldsymbol{\beta}\rangle_{\partial\mathcal{T}_h\setminus\Gamma} = -\langle\boldsymbol{n}\times\widehat{\delta}_{\boldsymbol{z}}^m + \tau_t(\widehat{\delta}_{\boldsymbol{u}}^m)^t,\boldsymbol{\beta}\rangle_{\partial\mathcal{T}_h\setminus\Gamma}, \tag{28}$$

$$\langle\varepsilon\boldsymbol{e}_{\widehat{\boldsymbol{u}}}^{n,m}\cdot\boldsymbol{n},\eta\rangle_{\partial\mathcal{T}_h^d} = -\langle\varepsilon\widehat{\delta}_{\boldsymbol{u}}^m\cdot\boldsymbol{n},\eta\rangle_{\partial\mathcal{T}_h^d}, \tag{29}$$

for all $(\boldsymbol{w},\boldsymbol{v},\psi,\boldsymbol{\beta},\eta) \in \mathcal{V}_h\times\mathcal{V}_h\times\mathcal{P}_h\times\mathcal{M}_h^t\times\Lambda_h$. In addition, $\boldsymbol{e}_{\widehat{\boldsymbol{u}}}^{t,m} \in \mathcal{M}_h^t(0)$.

Indeed, in (25) the terms $(\mu\widehat{\delta}_{\boldsymbol{z}}^m, \boldsymbol{w})_{\mathcal{T}_h}$, $(\widehat{\delta}_{\boldsymbol{u}}^m, \mathbf{curl}\,\boldsymbol{w})_{\mathcal{T}_h}$ and $\langle (\boldsymbol{u}^m)^t - \Pi_M^t(\boldsymbol{u}^m)^t, \boldsymbol{w}\times\boldsymbol{n}\rangle_{\partial\mathcal{T}_h}$ vanish by Lemma 8 $(i), (iii)$. In (26), Lemma 8 $(i), (ii)$ give

$$(\sigma(\partial_t\boldsymbol{u}(t_m) - \overline{\partial}_t\boldsymbol{u}_h^m), \boldsymbol{v})_{\mathcal{T}_h} = (\sigma\overline{\partial}_t\boldsymbol{e}_{\boldsymbol{u}}^m, \boldsymbol{v})_{\mathcal{T}_h} - (\sigma\widehat{\rho}_{\boldsymbol{u}}^m, \boldsymbol{v})_{\mathcal{T}_h} \quad \text{and}$$
$$(\widehat{\delta}_{\boldsymbol{z}}^m, \mathbf{curl}\,\boldsymbol{v})_{\mathcal{T}_h} = 0,$$

while a direct computation from (8) and (23) shows that

$$\boldsymbol{n}\times\boldsymbol{z}^m - \boldsymbol{n}\times\widehat{\boldsymbol{z}}_h^{t,m} = \boldsymbol{n}\times\boldsymbol{e}_{\widehat{\boldsymbol{z}}}^{t,m} + \boldsymbol{n}\times\widehat{\delta}_{\boldsymbol{z}}^m + \tau_t(\widehat{\delta}_{\boldsymbol{u}}^m)^t - \tau_t\big((\boldsymbol{u}^m)^t - \Pi_M^t(\boldsymbol{u}^m)^t\big),$$

whose last term is orthogonal to $\boldsymbol{v}$ and $\boldsymbol{\beta}$ by Lemma 8 $(iii)$; this also yields (28). Similarly, $\varepsilon\boldsymbol{u}^m\cdot\boldsymbol{n} - \varepsilon\widehat{\boldsymbol{u}}_h^{n,m}\cdot\boldsymbol{n} = \varepsilon\boldsymbol{e}_{\widehat{\boldsymbol{u}}}^{n,m}\cdot\boldsymbol{n} + \varepsilon\widehat{\delta}_{\boldsymbol{u}}^m\cdot\boldsymbol{n}$ and $(\varepsilon\widehat{\delta}_{\boldsymbol{u}}^m, \nabla\psi)_{\mathcal{T}_h^d} = 0$, which give (27) and (29). Finally, from the last equation of (7) and Lemma 8 $(iii)$, $\langle\boldsymbol{n}\times\boldsymbol{e}_{\widehat{\boldsymbol{u}}}^{t,m}, \boldsymbol{\beta}\rangle_\Gamma = \langle\boldsymbol{n}\times\boldsymbol{u}^m, \boldsymbol{\beta}\rangle_\Gamma - \langle\boldsymbol{g}^m, \boldsymbol{\beta}\rangle_\Gamma = 0$ for all $\boldsymbol{\beta}\in\mathcal{M}_h^t$, and hence $\boldsymbol{e}_{\widehat{\boldsymbol{u}}}^{t,m} = \boldsymbol{0}$ on $\Gamma$.

We note that, thanks to the use of $L^2$-projections and of piecewise constant coefficients, (25) is homogeneous, and the only spatial consistency terms are the face terms involving $\widehat{\delta}_{\boldsymbol{z}}^m$ and $\widehat{\delta}_{\boldsymbol{u}}^m$.

We now recall the discrete Gronwall's inequality in the form given in [24] (see also [30]).

**Lemma 9 (Discrete Gronwall's inequality)** *Let $\Delta t > 0$, $B \geq 0$, and let $a_m, b_m, \gamma_m \geq 0$ for $m \geq 1$ be such that*

$$a_\ell + \Delta t\sum_{m=1}^{\ell} b_m \leq \Delta t\sum_{m=1}^{\ell}\gamma_m a_m + B \qquad \forall\,\ell \geq 1.$$

*If $\forall\, m \geq 1 \,:\, \Delta t\,\gamma_m < 1$, then*

$$a_\ell + \Delta t\sum_{m=1}^{\ell} b_m \leq \exp\Big(\Delta t\sum_{m=1}^{\ell}\frac{\gamma_m}{1-\Delta t\,\gamma_m}\Big)B \qquad \forall\,\ell \geq 1.$$

**Lemma 10** *Let $(\boldsymbol{e}_{\boldsymbol{z}}^m, \boldsymbol{e}_{\boldsymbol{u}}^m, e_\varphi^m, \boldsymbol{e}_{\widehat{\boldsymbol{u}}}^{t,m}, \widehat{e}_\varphi^m)$ be the solution of the error system (25)–(29), and assume $\Delta t \leq 1/2$. Then, for each $\ell \in \{1,\dots,M\}$:*

$$\begin{aligned}\|\sqrt{\sigma}\boldsymbol{e}_{\boldsymbol{u}}^\ell\|_{\mathcal{T}_h}^2 + \Delta t\sum_{m=1}^{\ell}\Big(&\|\sqrt{\mu}\boldsymbol{e}_{\boldsymbol{z}}^m\|_{\mathcal{T}_h}^2 + \|e_\varphi^m\|_{\mathcal{T}_h^d}^2\\ &+ \tau_t\|(\boldsymbol{e}_{\boldsymbol{u}}^m)^t - \boldsymbol{e}_{\widehat{\boldsymbol{u}}}^{t,m}\|_{\partial\mathcal{T}_h}^2 + \tau_n\|e_\varphi^m - \widehat{e}_\varphi^m\|_{\partial\mathcal{T}_h^d}^2\Big)\\ &\leq e^{2T}\Big(\|\sqrt{\sigma}\boldsymbol{e}_{\boldsymbol{u}}^0\|_{\mathcal{T}_h}^2 + 2\Delta t\sum_{m=1}^{\ell}\Theta^m\Big),\end{aligned} \tag{30}$$

*where*

$$\begin{aligned}\Theta^m := \frac{1}{2}\|\sqrt{\sigma}\,\widehat{\rho}_{\boldsymbol{u}}^m\|_{\mathcal{T}_h}^2 + \overline{\mu}\,\|\boldsymbol{\xi}^m\|_{\mathcal{T}_h}^2 + \tau_t^{-1}\|\boldsymbol{\xi}^m - \Pi_V\boldsymbol{\xi}^m\|_{\partial\mathcal{T}_h}^2\\ + 2\tau_t^{-1}\|\widehat{\delta}_{\boldsymbol{z}}^m\|_{\partial\mathcal{T}_h}^2 + 2\tau_t\|\widehat{\delta}_{\boldsymbol{u}}^m\|_{\partial\mathcal{T}_h}^2 + \frac{\overline{\varepsilon}^2}{2\tau_n}\|\widehat{\delta}_{\boldsymbol{u}}^m\|_{\partial\mathcal{T}_h^d}^2.\end{aligned}$$

**Proof.** Fix $m \geq 1$ and set $\boldsymbol{E}_t := (\boldsymbol{e}_{\boldsymbol{u}}^m)^t - \boldsymbol{e}_{\widehat{\boldsymbol{u}}}^{t,m}$ and $E_n := e_\varphi^m - \widehat{e}_\varphi^m$. We select the test functions

$$\boldsymbol{w} = \boldsymbol{e}_{\boldsymbol{z}}^m, \qquad \boldsymbol{v} = \boldsymbol{e}_{\boldsymbol{u}}^m, \qquad \psi = e_\varphi^m, \qquad \boldsymbol{\beta} = -\boldsymbol{e}_{\widehat{\boldsymbol{u}}}^{t,m}, \qquad \eta = \widehat{e}_\varphi^m,$$

which are admissible since $\boldsymbol{e}_{\widehat{\boldsymbol{u}}}^{t,m} \in \mathcal{M}_h^t(0)$. Substituting these choices into (25)–(29), summing the resulting equations, and applying Lemma 3 to the left-hand side, yields

$$\begin{aligned}
&(\sigma \overline{\partial}_t \boldsymbol{e}_{\boldsymbol{u}}^m, \boldsymbol{e}_{\boldsymbol{u}}^m)_{\mathcal{T}_h} + \|\sqrt{\mu}\, \boldsymbol{e}_{\boldsymbol{z}}^m\|_{\mathcal{T}_h}^2 + \|e_\varphi^m\|_{\mathcal{T}_h^d}^2 + \tau_t \|\boldsymbol{E}_t\|_{\partial\mathcal{T}_h}^2 + \tau_n \|E_n\|_{\partial\mathcal{T}_h^d}^2 \\
&\quad = (\sigma \widehat{\rho}_{\boldsymbol{u}}^m, \boldsymbol{e}_{\boldsymbol{u}}^m)_{\mathcal{T}_h} + (\mathbf{curl}\, \boldsymbol{\xi}^m, \boldsymbol{e}_{\boldsymbol{u}}^m)_{\mathcal{T}_h} \\
&\qquad - \langle \boldsymbol{n} \times \widehat{\delta}_{\boldsymbol{z}}^m + \tau_t (\widehat{\delta}_{\boldsymbol{u}}^m)^t, \boldsymbol{E}_t \rangle_{\partial\mathcal{T}_h} + \langle \varepsilon \widehat{\delta}_{\boldsymbol{u}}^m \cdot \boldsymbol{n}, E_n \rangle_{\partial\mathcal{T}_h^d},
\end{aligned} \tag{31}$$

where we used that $\boldsymbol{n} \times \widehat{\delta}_{\boldsymbol{z}}^m$ and $(\widehat{\delta}_{\boldsymbol{u}}^m)^t$ are tangential.

In a similar way to (16) we obtain

$$(\sigma \overline{\partial}_t \boldsymbol{e}_{\boldsymbol{u}}^m, \boldsymbol{e}_{\boldsymbol{u}}^m)_{\mathcal{T}_h} \geq \frac{1}{2\Delta t} \Big( \|\sqrt{\sigma} \boldsymbol{e}_{\boldsymbol{u}}^m\|_{\mathcal{T}_h}^2 - \|\sqrt{\sigma} \boldsymbol{e}_{\boldsymbol{u}}^{m-1}\|_{\mathcal{T}_h}^2 \Big). \tag{32}$$

For the terms on the right-hand side of (31), we apply the Cauchy–Schwarz and Young inequalities. For the second one, we notice that, by (25) and $\boldsymbol{e}_{\widehat{\boldsymbol{u}}}^{t,m} \in \mathcal{M}_h^t(0)$, we can apply Lemma 5 with $\mathbf{a} = \boldsymbol{\xi}^m$ and $(\boldsymbol{p}_h, \boldsymbol{v}_h, \boldsymbol{\beta}_h) = (\boldsymbol{e}_{\boldsymbol{z}}^m, \boldsymbol{e}_{\boldsymbol{u}}^m, \boldsymbol{e}_{\widehat{\boldsymbol{u}}}^{t,m})$. We have:

$$\begin{aligned}
&|(\sigma \widehat{\rho}_{\boldsymbol{u}}^m, \boldsymbol{e}_{\boldsymbol{u}}^m)_{\mathcal{T}_h}| \leq \frac{1}{2} \|\sqrt{\sigma}\, \widehat{\rho}_{\boldsymbol{u}}^m\|_{\mathcal{T}_h}^2 + \frac{1}{2} \|\sqrt{\sigma}\, \boldsymbol{e}_{\boldsymbol{u}}^m\|_{\mathcal{T}_h}^2, \\
&|(\mathbf{curl}\, \boldsymbol{\xi}^m, \boldsymbol{e}_{\boldsymbol{u}}^m)_{\mathcal{T}_h}| \leq \frac{1}{4} \|\sqrt{\mu}\, \boldsymbol{e}_{\boldsymbol{z}}^m\|_{\mathcal{T}_h}^2 + \overline{\mu}\, \|\boldsymbol{\xi}^m\|_{\mathcal{T}_h}^2 \\
&\qquad + \frac{\tau_t}{4} \|\boldsymbol{E}_t\|_{\partial\mathcal{T}_h}^2 + \tau_t^{-1} \|\boldsymbol{\xi}^m - \Pi_V \boldsymbol{\xi}^m\|_{\partial\mathcal{T}_h}^2, \\
&|\langle \boldsymbol{n} \times \widehat{\delta}_{\boldsymbol{z}}^m + \tau_t (\widehat{\delta}_{\boldsymbol{u}}^m)^t, \boldsymbol{E}_t \rangle_{\partial\mathcal{T}_h}| \leq \frac{\tau_t}{4} \|\boldsymbol{E}_t\|_{\partial\mathcal{T}_h}^2 \\
&\qquad + 2\tau_t^{-1} \|\widehat{\delta}_{\boldsymbol{z}}^m\|_{\partial\mathcal{T}_h}^2 + 2\tau_t \|\widehat{\delta}_{\boldsymbol{u}}^m\|_{\partial\mathcal{T}_h}^2, \\
&|\langle \varepsilon \widehat{\delta}_{\boldsymbol{u}}^m \cdot \boldsymbol{n}, E_n \rangle_{\partial\mathcal{T}_h^d}| \leq \frac{\tau_n}{2} \|E_n\|_{\partial\mathcal{T}_h^d}^2 + \frac{\overline{\varepsilon}^2}{2\tau_n} \|\widehat{\delta}_{\boldsymbol{u}}^m\|_{\partial\mathcal{T}_h^d}^2.
\end{aligned} \tag{33}$$

Substituting (32) and (33) into (31), multiplying by $2\Delta t$, summing up from $m = 1$ to $m = \ell$, and after applying telescopic property, we obtain

$$\begin{aligned}
&\|\sqrt{\sigma}\, \boldsymbol{e}_{\boldsymbol{u}}^\ell\|_{\mathcal{T}_h}^2 + \Delta t \sum_{m=1}^{\ell} \Big( \frac{3}{2} \|\sqrt{\mu}\, \boldsymbol{e}_{\boldsymbol{z}}^m\|_{\mathcal{T}_h}^2 + 2\|e_\varphi^m\|_{\mathcal{T}_h^d}^2 + \tau_t \|\boldsymbol{E}_t\|_{\partial\mathcal{T}_h}^2 + \tau_n \|E_n\|_{\partial\mathcal{T}_h^d}^2 \Big) \\
&\leq \Delta t \sum_{m=1}^{\ell} \|\sqrt{\sigma}\, \boldsymbol{e}_{\boldsymbol{u}}^m\|_{\mathcal{T}_h}^2 + \|\sqrt{\sigma}\, \boldsymbol{e}_{\boldsymbol{u}}^0\|_{\mathcal{T}_h}^2 + 2\Delta t \sum_{m=1}^{\ell} \Theta^m.
\end{aligned} \tag{34}$$

We now apply Lemma 9 to (34) with $a_m = \|\sqrt{\sigma}\, \boldsymbol{e}_{\boldsymbol{u}}^m\|_{\mathcal{T}_h}^2$, $\gamma_m = 1$, $b_m$ the term in parentheses, and $B = \|\sqrt{\sigma}\, \boldsymbol{e}_{\boldsymbol{u}}^0\|_{\mathcal{T}_h}^2 + 2\Delta t \sum_{m=1}^{\ell} \Theta^m$ (for fixed $\ell$, $B$ bounds the right-hand side of (34) for all $\ell' \leq \ell$). Since $\Delta t \leq 1/2$, we have $(1 - \Delta t)^{-1} \leq 2$, and the exponential factor is bounded by $\exp(2\ell\Delta t) \leq e^{2T}$. This proves (30). $\square$

**Theorem 11** *Assume that the exact solution and the source satisfy*

$$\boldsymbol{z} \in H^1(0,T;[H^{k+1}(\mathcal{T}_h)]^3), \quad \boldsymbol{u} \in H^1(0,T;[H^{k+1}(\mathcal{T}_h)]^3),$$

$$\boldsymbol{u}|_{\Omega_{\mathtt{c}}} \in H^2(0,T;[L^2(\Omega_{\mathtt{c}})]^3), \quad \mathbf{H}_{\mathtt{s}} \in H^2(0,T;[H^1(\Omega)]^3),$$

*and choose the stabilization parameters $\tau_t \sim 1$ and $\tau_n \sim 1$, and $\Delta t \le 1/2$. Then, there exists a constant $C > 0$, independent of $h$ and $\Delta t$, such that*

$$\begin{aligned}\max_{1\le m\le M} \|\sqrt{\sigma}\,(\boldsymbol{u}(t_m) - \boldsymbol{u}_h^m)\|_{\mathcal{T}_h} + \left(\Delta t \sum_{m=1}^{M} \|\boldsymbol{z}(t_m) - \boldsymbol{z}_h^m\|_{\mathcal{T}_h}^2\right)^{1/2} \\ + \left(\Delta t \sum_{m=1}^{M} \|\varphi(t_m) - \varphi_h^m\|_{\mathcal{T}_h^d}^2\right)^{1/2} \le C(h^{k+1/2} + \Delta t).\end{aligned} \tag{35}$$

**Proof.** The result follows from Lemma 10, the approximation properties of Lemma 8, and standard estimates for the temporal consistency errors (22). We bound the terms on the right-hand side of (30).

For the initial error, since $\boldsymbol{u}(0) = \boldsymbol{u}_0$ in $\Omega_{\mathtt{c}}$ and $\Pi_V$ acts elementwise, we have $\sqrt{\sigma}\,\boldsymbol{e}_{\boldsymbol{u}}^0 = \sqrt{\sigma}\,(\Pi_V\boldsymbol{u}(0) - \Pi_V\boldsymbol{u}_0) = \mathbf{0}$.

For the temporal consistency term $\widehat{\rho}_{\boldsymbol{u}}^m$, Taylor expansion with integral remainder yields

$$\widehat{\rho}_{\boldsymbol{u}}^m = \overline{\partial}_t\boldsymbol{u}^m - \partial_t\boldsymbol{u}(t_m) = \frac{1}{\Delta t}\int_{t_{m-1}}^{t_m} (t_{m-1} - s)\partial_{tt}\boldsymbol{u}(s)\,ds,$$

whence

$$\|\widehat{\rho}_{\boldsymbol{u}}^m\|_{\Omega_{\mathtt{c}}}^2 \le \frac{\Delta t}{3}\|\partial_{tt}\boldsymbol{u}\|_{L^2(t_{m-1},t_m;[L^2(\Omega_{\mathtt{c}})]^3)}^2,$$

and then, since $\sigma = 0$ in $\Omega_{\mathtt{d}}$,

$$\Delta t \sum_{m=1}^{M} \|\sqrt{\sigma}\,\widehat{\rho}_{\boldsymbol{u}}^m\|_{\mathcal{T}_h}^2 \le \frac{\overline{\sigma}\,\Delta t^2}{3}\|\partial_{tt}\boldsymbol{u}\|_{L^2(0,T;[L^2(\Omega_{\mathtt{c}})]^3)}^2.$$

In the same way, $\Delta t\sum_{m=1}^{M}\|\boldsymbol{\xi}^m\|_{H^1(\Omega)}^2 \le \frac{\Delta t^2}{3}\|\partial_{tt}\mathbf{H}_{\mathtt{s}}\|_{L^2(0,T;[H^1(\Omega)]^3)}^2$ and, by (21b) with $s = 1$, $\|\boldsymbol{\xi}^m - \Pi_V\boldsymbol{\xi}^m\|_{\partial\mathcal{T}_h}^2 \le C\,h\,|\boldsymbol{\xi}^m|_{H^1(\Omega)}^2$. Therefore,

$$\Delta t \sum_{m=1}^{M} \left(\overline{\mu}\,\|\boldsymbol{\xi}^m\|_{\mathcal{T}_h}^2 + \tau_t^{-1}\|\boldsymbol{\xi}^m - \Pi_V\boldsymbol{\xi}^m\|_{\partial\mathcal{T}_h}^2\right) \le C\,\Delta t^2.$$

For the spatial consistency terms, (21b) with $s = k+1$ gives

$$\begin{aligned}\|\widehat{\delta}_{\boldsymbol{z}}^m\|_{\partial\mathcal{T}_h}^2 + \|\widehat{\delta}_{\boldsymbol{u}}^m\|_{\partial\mathcal{T}_h}^2 \le C\,h^{2k+1}\Big(&|\boldsymbol{z}(t_m)|_{H^{k+1}(\mathcal{T}_h)}^2 \\ &+ |\boldsymbol{u}(t_m)|_{H^{k+1}(\mathcal{T}_h)}^2\Big),\end{aligned}$$

and, since $H^1(0,T;[H^{k+1}(\mathcal{T}_h)]^3) \subset C([0,T];[H^{k+1}(\mathcal{T}_h)]^3)$, we get

$$\Delta t \sum_{m=1}^{M} \big( \|\widehat{\delta}_{\boldsymbol{z}}^m\|_{\partial\mathcal{T}_h}^2 + \|\widehat{\delta}_{\boldsymbol{u}}^m\|_{\partial\mathcal{T}_h}^2 \big) \le C\, h^{2k+1}.$$

Substituting these bounds into (30), we obtain

$$\max_{1\le m\le M} \|\sqrt{\sigma}\, \boldsymbol{e}_{\boldsymbol{u}}^m\|_{\mathcal{T}_h}^2 + \Delta t \sum_{m=1}^{M} \Big( \|\sqrt{\mu}\, \boldsymbol{e}_{\boldsymbol{z}}^m\|_{\mathcal{T}_h}^2 + \|e_\varphi^m\|_{\mathcal{T}_h^d}^2 \Big) \le C\big(h^{2k+1} + \Delta t^2\big).$$

Finally, we write $\boldsymbol{u}(t_m) - \boldsymbol{u}_h^m = \widehat{\delta}_{\boldsymbol{u}}^m + \boldsymbol{e}_{\boldsymbol{u}}^m$, $\boldsymbol{z}(t_m) - \boldsymbol{z}_h^m = \widehat{\delta}_{\boldsymbol{z}}^m + \boldsymbol{e}_{\boldsymbol{z}}^m$ and $\varphi(t_m) - \varphi_h^m = e_\varphi^m$, and use (21a), which gives $\|\widehat{\delta}_{\boldsymbol{u}}^m\|_{\mathcal{T}_h} + \|\widehat{\delta}_{\boldsymbol{z}}^m\|_{\mathcal{T}_h} \le C\, h^{k+1}$. This yields (35). □

**Remark 12** *The estimate* (35) *is optimal in time, but suboptimal by $h^{1/2}$ in space. This loss comes from the face terms in* (26)–(29)*, which do not vanish for $L^2$-projections. Recovering the rate $h^{k+1}$ would require an HDG projection adapted to the curl–curl structure of the problem, for which these face terms vanish (in the spirit of the projections introduced in [21] for diffusion problems, and of the projection-based analysis of [23] for the static Maxwell equations); the construction of such a projection is left for future work.*

**Remark 13** *The form $\mathbf{J} = \mathbf{curl}\,\mathbf{H}_{\mathtt{s}}$ is needed only in $\Omega_{\mathtt{d}}$, where* (30) *gives no $L^2$ control of $\boldsymbol{e}_{\boldsymbol{u}}^m$. Let $\mathbf{J} = \mathbf{curl}\,\mathbf{H}_{\mathtt{s}} + \mathbf{J}_{\mathtt{c}}$, with $\mathbf{H}_{\mathtt{s}}$ as in Theorem 11 and $\mathbf{J}_{\mathtt{c}} \in H^2(0,T;[L^2(\Omega_{\mathtt{c}})]^3)$ extended by zero to $\Omega_{\mathtt{d}}$. Proposition 2 still holds, since the function $\nabla\widetilde{\psi}$ in its proof vanishes in $\Omega_{\mathtt{c}}$. The term $\boldsymbol{\zeta}^m := \overline{\partial}_t \mathbf{J}_{\mathtt{c}}^m - \partial_t \mathbf{J}_{\mathtt{c}}(t_m)$ is added to the right-hand side of* (26)*, and it is bounded together with $\sigma\widehat{\rho}_{\boldsymbol{u}}^m$ in the first line of* (33)*. Hence* (35) *holds, with a constant that also depends on $\partial_{tt}\mathbf{J}_{\mathtt{c}}$.*

*This class contains every $\mathbf{J} \in H^2(0,T;[L^2(\Omega)]^3)$ such that $\operatorname{div}\mathbf{J} = 0$ in $\Omega_{\mathtt{d}}$ and the flux of $\mathbf{J}|_{\Omega_{\mathtt{d}}}$ through $\Gamma_0$ vanishes, which are the compatibility conditions of [5]. Indeed, such a restriction is the curl of a field in $H^2(0,T;[H^1(\Omega_{\mathtt{d}})]^3)$, by [9] and a bounded linear right inverse of the curl on divergence-free fields with vanishing fluxes, and that field extends to $\Omega$.*

# 5 Numerical results

In this section we illustrate the performance of the fully discrete HDG scheme (7)–(8). In Example 1 (Section 5.1) we test Theorem 11 with a manufactured solution that satisfies its assumptions, and in Example 2 (Section 5.2) we repeat the experiments with a source in the class of Remark 13. In Example 3 (Section 5.3) we remove the time discretization error in order to measure the spatial order alone; and in Example 4 (Section 5.4) we apply the method to a model problem of magnetic shielding by eddy currents, for which no closed-form solution is available.

The method has been implemented in MATLAB. On each element we use scaled monomial basis, and on each face a basis of $\mathbb{P}_k(F)$ for each component of $\widehat{\boldsymbol{u}}_h^t$ with respect to an orthonormal pair of tangent vectors. Volume and face integrals are computed with collapsed Gauss rules, which are exact for the polynomial integrands of the local matrices. The local unknowns $(\boldsymbol{z}_h^m, \boldsymbol{u}_h^m, \varphi_h^m)$ are eliminated element by element (static condensation), so that the global system only involves $\widehat{\boldsymbol{u}}_h^{t,m}$ and $\widehat{\varphi}_h^m$. Since $\widehat{\varphi}_h^m$ is fixed to zero on $\Gamma$ and to a single unknown constant on $\Gamma_0$, the latter adds only one scalar unknown to the global system.

The condensed matrix is symmetric, indefinite and independent of $m$; it is factorized once (by an $LDL^{\mathtt{t}}$ factorization) and the factors are reused at every time step.

In all the examples, $\Omega = (0,1)^3$, the conductor is the cube $\Omega_{\mathtt{c}} = (0.2, 0.8)^3$, and $\Omega_{\mathtt{d}} = \Omega \setminus \Omega_{\mathtt{c}}$. We take

$$\mu = 1 \text{ in } \Omega, \qquad \varepsilon = 1 \text{ in } \Omega, \qquad \sigma = 10 \text{ in } \Omega_{\mathtt{c}},$$
$$\sigma = 0 \text{ in } \Omega_{\mathtt{d}}, \qquad \tau_t = \tau_n = 1, \qquad T = 1.$$

We use the structured tetrahedral meshes described in Table 1, obtained by subdividing $\Omega$ into $N^3$ cubes and each cube into six tetrahedra; all of them are conforming with the interface $\Gamma_0$.

Table 1: Meshes used in the numerical experiments: number $N$ of cubes per direction, number of tetrahedra, mesh size $h$, and size of the condensed global system.

| | | | | Global unknowns | | |
|---|---|---|---|---|---|---|
| Mesh | $N$ | Elements | $h$ | $k=0$ | $k=1$ | $k=2$ |
| 1 | 5 | 750 | 0.3464 | 3 673 | 11 017 | 22 033 |
| 2 | 10 | 6 000 | 0.1732 | 31 393 | 94 177 | 188 353 |
| 3 | 15 | 20 250 | 0.1155 | 108 217 | 324 649 | 649 297 |
| 4 | 20 | 48 000 | 0.0866 | 259 201 | 777 601 | 1 555 201 |

In all the examples with a manufactured solution (Examples 1, 2 and 3), the errors are measured as follows. We report the quantities appearing in (35), in relative form:

$$E_{\boldsymbol{u}} := \frac{\max_m \|\sqrt{\sigma}(\boldsymbol{u}(t_m) - \boldsymbol{u}_h^m)\|_{\mathcal{T}_h}}{\max_m \|\sqrt{\sigma}\,\boldsymbol{u}(t_m)\|_{\mathcal{T}_h}}, \qquad E_{\boldsymbol{z}} := \left( \frac{\sum_m \|\boldsymbol{z}(t_m) - \boldsymbol{z}_h^m\|^2_{\mathcal{T}_h}}{\sum_m \|\boldsymbol{z}(t_m)\|^2_{\mathcal{T}_h}} \right)^{1/2},$$

and, since $\varphi = 0$, the absolute error $E_\varphi := \big(\Delta t \sum_m \|\varphi_h^m\|^2_{\mathcal{T}_h^d}\big)^{1/2}$. All maxima and sums are taken over $1 \le m \le M$. The experimental orders of convergence are

$$r_{\Delta t} := \frac{\log(E_i/E_{i+1})}{\log(\Delta t_i/\Delta t_{i+1})},$$
$$r_h := \frac{\log(E_i/E_{i+1})}{\log(h_i/h_{i+1})},$$

for two consecutive time steps on a fixed mesh, or two consecutive meshes with a fixed time step, respectively. We also monitored the discrete flux $\sum_{F \in \mathcal{E}_h^{\Gamma_0}} \int_F \varepsilon \widehat{\boldsymbol{u}}_h^{n,m} \cdot \boldsymbol{n}$: in all the runs of Examples 1–3 it was below $2 \times 10^{-14}$, that is, the discrete counterpart of the flux condition on $\Gamma_0$ holds up to round-off.

### 5.1 Example 1: a source of the form $\mathbf{J} = \mathbf{curl}\,\mathbf{H}_{\mathtt{s}}$

We first consider an exact solution for which the source is of the form $\mathbf{J} = \mathbf{curl}\,\mathbf{H}_{\mathtt{s}}$ assumed in Section 2 and used in the proof of Theorem 11. Let $a := \pi/0.6$, $p(s) := \sin\big(a(s-0.2)\big)$, $\widetilde{\psi}(\boldsymbol{x}) := p(x)\,p(y)\,p(z)$ and $\widetilde{\boldsymbol{U}} := \mathbf{curl}(0,0,\widetilde{\psi})$. The function $\widetilde{\psi}$ vanishes on $\Gamma_0$, since $p(0.2) = p(0.8) = 0$; consequently, $\widetilde{\boldsymbol{U}} \cdot \boldsymbol{n}_0 = 0$ on $\Gamma_0$. Moreover, $\operatorname{div} \widetilde{\boldsymbol{U}} = 0$ and, since $-\triangle\widetilde{\psi} = 3a^2\widetilde{\psi}$, $\mathbf{curl}\,\mathbf{curl}\,\widetilde{\boldsymbol{U}} = 3a^2\widetilde{\boldsymbol{U}}$. We take the exact solution

$$\boldsymbol{u}(t,\boldsymbol{x}) = g(t)\,\widetilde{\boldsymbol{U}}(\boldsymbol{x}), \qquad \boldsymbol{z} = \mu^{-1}\,\mathbf{curl}\,\boldsymbol{u}, \qquad \varphi = 0, \tag{36}$$

with $g(t) = 1 + \sin(2\pi t)$, and the source

$$\begin{aligned}
\mathbf{J}(t,\boldsymbol{x}) &= -\Big(\sigma\, g(t) + 3a^2\mu^{-1}G(t)\Big)\widetilde{\boldsymbol{U}}(\boldsymbol{x}) = \mathbf{curl}\,\mathbf{H}_{\mathtt{s}}(t,\boldsymbol{x}),\\
G(t) &= \int_0^t g(s)\,ds,\\
\mathbf{H}_{\mathtt{s}}(t,\boldsymbol{x}) &= -\Big(\sigma\, g(t) + 3a^2\mu^{-1}G(t)\Big)\big(0,0,\widetilde{\psi}(\boldsymbol{x})\big).
\end{aligned}$$

Indeed, $\sigma$ is constant in $\Omega_{\mathtt{c}}$ and in $\Omega_{\mathtt{d}}$, and $\mathbf{H}_{\mathtt{s}}$ is continuous across $\Gamma_0$ because $\widetilde{\psi} = 0$ there; hence $\mathbf{H}_{\mathtt{s}} \in H^2(0,T;[H^1(\Omega)]^3)$ and its curl has no singular part on $\Gamma_0$. The boundary datum $\boldsymbol{g} = \boldsymbol{n} \times \boldsymbol{u}$ on $\Gamma$, which does not vanish, and the initial datum are computed from $\boldsymbol{u}$, and $(\boldsymbol{z}, \boldsymbol{u}, 0)$ is the exact solution of (4). Thus this example satisfies the assumptions of Theorem 11.

For each mesh of Table 1 and each $k \in \{0,1,2\}$, we computed the solution with $\Delta t = 0.1{\cdot}2^{-j}$, $j = 0,\dots,4$. According to (35), the error is bounded by $C_1 h^{k+1/2} + C_2\Delta t$, and which of the two terms dominates depends on $k$.

Table 2 shows the results for $k = 2$ on mesh 4. For $k = 2$ the spatial part of the error is negligible on the finer meshes (on meshes 3 and 4 the errors $E_{\boldsymbol{u}}$ and $E_{\boldsymbol{z}}$ differ by at most 2%), and the scheme is of first order in $\Delta t$. For $k = 1$ the same behavior is observed while the temporal part dominates; for instance, on mesh 4 the orders of $E_{\boldsymbol{z}}$ are 0.96, 0.94 and 0.85.

Table 2: Example 1: relative errors and orders of convergence in $\Delta t$.

| | $\Delta t$ | $E_{\boldsymbol{u}}$ | $r_{\Delta t}$ | $E_{\boldsymbol{z}}$ | $r_{\Delta t}$ |
|---|---|---|---|---|---|
| $k = 2$ mesh 4 | 0.1 | 1.22e-01 | – | 1.23e-01 | – |
| | 0.05 | 6.30e-02 | 0.96 | 6.26e-02 | 0.97 |
| | 0.025 | 3.25e-02 | 0.96 | 3.17e-02 | 0.98 |
| | 0.0125 | 1.65e-02 | 0.98 | 1.59e-02 | 0.99 |
| | 0.00625 | 8.35e-03 | 0.98 | 7.99e-03 | 0.99 |

Table 3 shows the errors for $\Delta t = 0.00625$. For $k = 0$ the errors are essentially independent of $\Delta t$ (for $\Delta t \le 0.025$, $E_{\boldsymbol{u}}$ and $E_\varphi$ change by less than 1%, and $E_{\boldsymbol{z}}$ by less than 4%). The relative errors are large on the coarse meshes, since piecewise constants resolve $\widetilde{\psi}$, which completes a half period across the conductor, only on fine meshes; nevertheless, all the orders are above the rate $h^{1/2}$ guaranteed by Theorem 11. Those of $E_{\boldsymbol{u}}$ and $E_{\boldsymbol{z}}$ increase towards $1 = k+1$, and those of $E_\varphi$ exceed 1. For $k = 1$, $E_{\boldsymbol{u}}$ and $E_\varphi$ converge with order close to $2 = k+1$, above the guaranteed rate $h^{3/2}$, and so does $E_{\boldsymbol{z}}$ up to mesh 3; between meshes 3 and 4 its temporal part, which is about $8 \times 10^{-3}$ for this $\Delta t$ (Table 2), is no longer negligible. The model $E \approx \big((A\,h^p)^2 + (B\,\Delta t)^2\big)^{1/2}$, fitted to the 20 values of each error for $k = 1$, gives $p = 1.85$ for $E_{\boldsymbol{u}}$ and $p = 1.90$ for $E_{\boldsymbol{z}}$, with maximum relative deviations of 10% and 2%, respectively. For $k = 2$, the error $E_\varphi$, which is not affected by the time discretization, converges with orders 3.01, 2.91 and 2.90 between consecutive meshes. The discrete flux on $\Gamma_0$ was below $2 \times 10^{-14}$ in all the runs. Therefore, the experiments are consistent with Theorem 11: the scheme is of first order in $\Delta t$, and the spatial part of the error decreases at least with order $k + 1/2$, and with order close to $k + 1$ for $k = 1, 2$.

Table 3: Example 1: errors and orders of convergence in $h$ for $\Delta t = 0.00625$. †: the temporal part of the error is not negligible.

| | mesh | $h$ | $E_{\boldsymbol{u}}$ | $r_h$ | $E_{\boldsymbol{z}}$ | $r_h$ | $E_\varphi$ | $r_h$ |
|---|---|---|---|---|---|---|---|---|
| $k=0$ | 1 | 0.3464 | 1.27e+00 | – | 5.43e-01 | – | 1.16e+00 | – |
| | 2 | 0.1732 | 8.09e-01 | 0.66 | 3.17e-01 | 0.78 | 4.54e-01 | 1.35 |
| | 3 | 0.1155 | 5.87e-01 | 0.79 | 2.24e-01 | 0.85 | 2.54e-01 | 1.43 |
| | 4 | 0.0866 | 4.59e-01 | 0.85 | 1.74e-01 | 0.88 | 1.72e-01 | 1.36 |
| $k=1$ | 1 | 0.3464 | 3.87e-01 | – | 1.25e-01 | – | 2.53e-01 | – |
| | 2 | 0.1732 | 1.17e-01 | 1.73 | 3.46e-02 | 1.86 | 6.84e-02 | 1.89 |
| | 3 | 0.1155 | 5.41e-02 | 1.89 | 1.73e-02 | 1.70 | 2.83e-02 | 2.18 |
| | 4 | 0.0866 | 3.09e-02 | 1.94 | 1.19e-02 | $1.31^\dagger$ | 1.52e-02 | 2.16 |

### 5.2 Example 2: convergence in time and space

We now consider a source that is not a curl in $\Omega$, but that belongs to the class of Remark 13. Let $\psi(\boldsymbol{x}) = \sin(\pi x)\sin(\pi y)\sin(\pi z)$ and $\boldsymbol{U} := \mathbf{curl}(0,0,\psi)$. Then $\operatorname{div}\boldsymbol{U} = 0$ and $\mathbf{curl}\,\mathbf{curl}\,\boldsymbol{U} = 3\pi^2\boldsymbol{U}$. We take the exact solution

$$\boldsymbol{u}(t,\boldsymbol{x}) = g(t)\,\boldsymbol{U}(\boldsymbol{x}), \qquad \boldsymbol{z} = \mu^{-1}\,\mathbf{curl}\,\boldsymbol{u}, \qquad \varphi = 0, \tag{37}$$

with $g(t) = 1 + \sin(2\pi t)$, and the source

$$\mathbf{J}(t,\boldsymbol{x}) = -\Big(\sigma\, g(t) + 3\pi^2\mu^{-1}G(t)\Big)\boldsymbol{U}(\boldsymbol{x}), \qquad G(t) = \int_0^t g(s)\,ds,$$

so that $\sigma\partial_t\boldsymbol{u} + \mathbf{curl}(\mu^{-1}\,\mathbf{curl}\,\boldsymbol{u}) = -\partial_t\mathbf{J}$ in $\Omega$. The boundary datum $\boldsymbol{g} = \boldsymbol{n}\times\boldsymbol{u}$ on $\Gamma$ and the initial datum $\boldsymbol{u}_0 = \boldsymbol{U}$ are computed from $\boldsymbol{u}$. Since $\operatorname{div}(\varepsilon\boldsymbol{u}) = 0$ in $\Omega_{\mathtt{d}}$ and $\langle\varepsilon\boldsymbol{u}\cdot\boldsymbol{n}_0, 1\rangle_{\Gamma_0} = 0$, the triple $(\boldsymbol{z},\boldsymbol{u},0)$ is the exact solution of (4). Since the normal component of $\mathbf{J}$ jumps across $\Gamma_0$, $\mathbf{J}$ is not of the form $\mathbf{curl}\,\mathbf{H}_{\mathtt{s}}$. It belongs to the class of Remark 13, with $\mathbf{H}_{\mathtt{s}} = -3\pi^2\mu^{-1}G(t)\,(0,0,\psi)$ and $\mathbf{J}_{\mathtt{c}} = -\sigma g(t)\boldsymbol{U}$. As shown below, the observed orders are similar to those of Example 1. As in (7), the source enters the scheme through $\overline{\partial}_t\mathbf{J}^m$.

For each mesh and each $k \in \{0,1,2\}$, we computed the solution with $\Delta t = 0.1\cdot 2^{-j}$, $j = 0,\dots,4$. According to (35), the error is bounded by $C_1 h^{k+1/2} + C_2\Delta t$, and which of the two terms dominates depends on $k$. For $k = 2$ the spatial part is negligible already on mesh 2: on meshes 2 to 4 the errors $E_{\boldsymbol{u}}$ and $E_{\boldsymbol{z}}$ differ by less than 2%, so that they measure the time discretization error alone. Table 4 shows the results on mesh 4: the scheme is of first order in $\Delta t$, as predicted by Theorem 11 and Remark 13. For $k = 1$ the order of $E_{\boldsymbol{u}}$ decreases for the smallest time step, because the error approaches its spatial part, which is no longer negligible compared with the temporal one.

Table 4: Example 2: relative errors and orders of convergence in $\Delta t$.

| | $\Delta t$ | $E_{\boldsymbol{u}}$ | $r_{\Delta t}$ | $E_{\boldsymbol{z}}$ | $r_{\Delta t}$ |
|---|---|---|---|---|---|
| $k=1$ mesh 4 | 0.1 | 7.17e-02 | – | 9.27e-02 | – |
| | 0.05 | 3.72e-02 | 0.95 | 4.77e-02 | 0.96 |
| | 0.025 | 1.95e-02 | 0.93 | 2.44e-02 | 0.97 |
| | 0.0125 | 1.05e-02 | 0.89 | 1.26e-02 | 0.96 |
| | 0.00625 | 8.02e-03 | 0.39 | 6.80e-03 | 0.89 |
| $k=2$ mesh 4 | 0.1 | 7.13e-02 | – | 9.26e-02 | – |
| | 0.05 | 3.67e-02 | 0.96 | 4.76e-02 | 0.96 |
| | 0.025 | 1.89e-02 | 0.96 | 2.42e-02 | 0.98 |
| | 0.0125 | 9.60e-03 | 0.98 | 1.22e-02 | 0.99 |
| | 0.00625 | 4.84e-03 | 0.99 | 6.11e-03 | 0.99 |

For $k=0$ the situation is the opposite: the spatial part dominates and, for $\Delta t \le 0.025$, the errors $E_{\boldsymbol{u}}$ and $E_\varphi$ change by less than 1% on all the meshes ($E_{\boldsymbol{z}}$ by less than 7%), so that they can be used to measure the order in $h$. For $k=1$ both parts are of the same size on the finer meshes. Table 5 shows the errors for $\Delta t = 0.00625$. For $k=0$ all the orders are above the rate $h^{1/2}$ guaranteed by Remark 13. Those of $E_{\boldsymbol{u}}$ and $E_{\boldsymbol{z}}$ increase towards $1 = k+1$, and those of $E_\varphi$ exceed 1. For $k=1$, $E_{\boldsymbol{u}}$ and $E_\varphi$ converge with order close to $2 = k+1$, again above the guaranteed rate $h^{3/2}$. For $E_{\boldsymbol{z}}$, instead, the temporal part of the error, which is about $6 \times 10^{-3}$ for this $\Delta t$ (Table 4), dominates on meshes 3 and 4, so that its order in $h$ cannot be read from Table 5. To separate both contributions for $k=1$, we fitted the model $E \approx \left((A\,h^p)^2 + (B\,\Delta t)^2\right)^{1/2}$ to the 20 values (four meshes and five time steps) of each error by nonlinear least squares, and obtained $p = 1.93$ for $E_{\boldsymbol{u}}$ and $p = 1.88$ for $E_{\boldsymbol{z}}$, with maximum relative deviations of 10% and 3%, respectively.

Table 5: Example 2: errors and orders of convergence in $h$ for $\Delta t = 0.00625$. †: the temporal part of the error dominates.

| | mesh | $h$ | $E_{\boldsymbol{u}}$ | $r_h$ | $E_{\boldsymbol{z}}$ | $r_h$ | $E_\varphi$ | $r_h$ |
|---|---|---|---|---|---|---|---|---|
| $k=0$ | 1 | 0.3464 | 4.58e-01 | – | 3.05e-01 | – | 2.55e-01 | – |
| | 2 | 0.1732 | 2.86e-01 | 0.68 | 1.72e-01 | 0.82 | 1.21e-01 | 1.08 |
| | 3 | 0.1155 | 2.08e-01 | 0.79 | 1.21e-01 | 0.87 | 7.59e-02 | 1.15 |
| | 4 | 0.0866 | 1.63e-01 | 0.85 | 9.42e-02 | 0.88 | 5.44e-02 | 1.16 |
| $k=1$ | 1 | 0.3464 | 1.04e-01 | – | 4.23e-02 | – | 3.78e-02 | – |
| | 2 | 0.1732 | 3.00e-02 | 1.79 | 1.27e-02 | 1.74 | 1.09e-02 | 1.79 |
| | 3 | 0.1155 | 1.39e-02 | 1.90 | 7.99e-03 | $1.14^\dagger$ | 4.75e-03 | 2.05 |
| | 4 | 0.0866 | 8.02e-03 | 1.91 | 6.80e-03 | $0.56^\dagger$ | 2.64e-03 | 2.04 |

### 5.3 Example 3: convergence in space

To measure the spatial order without the influence of the time discretization, we take (37) (the solution of Example 2) with $g(t) = 1+t$, and replace $\overline{\partial}_t \mathbf{J}^m$ by $\partial_t \mathbf{J}(t_m)$ in (7). Since $\boldsymbol{u}$ is linear in $t$, $\overline{\partial}_t \boldsymbol{u}(t_m) = \partial_t \boldsymbol{u}(t_m)$,

so that the exact solution satisfies the time-discrete equations exactly, and the error is only due to the spatial discretization. Accordingly, when $\Delta t$ goes from 0.1 to 0.05 the errors change by less than 0.2% (by 1.6% for $E_\varphi$, whose definition involves a sum in time). Table 6 shows the results for $k = 2$ and $\Delta t = 0.05$. All the errors, including $E_{\boldsymbol{u}}$ and $E_{\boldsymbol{z}}$, converge with order close to $3 = k + 1$, above the rate $h^{5/2}$ of Theorem 11.

Table 6: Example 3 ($g(t) = 1 + t$, no time discretization error): errors and orders of convergence in $h$ for $\Delta t = 0.05$.

| | mesh | $h$ | $E_{\boldsymbol{u}}$ | $r_h$ | $E_{\boldsymbol{z}}$ | $r_h$ | $E_\varphi$ | $r_h$ |
|---|---|---|---|---|---|---|---|---|
| $k = 2$ | 1 | 0.3464 | 1.18e-02 | – | 4.21e-03 | – | 5.51e-03 | – |
| | 2 | 0.1732 | 1.65e-03 | 2.85 | 5.42e-04 | 2.96 | 7.30e-04 | 2.92 |
| | 3 | 0.1155 | 4.99e-04 | 2.95 | 1.62e-04 | 2.98 | 2.25e-04 | 2.91 |
| | 4 | 0.0866 | 2.12e-04 | 2.98 | 6.83e-05 | 2.99 | 9.70e-05 | 2.92 |

The experiment above uses the source of Example 2. To complete the picture, we also repeated it with the function $\widetilde{\psi}$ of Example 1, that is, with $\boldsymbol{u}(t, \boldsymbol{x}) = (1 + t)\,\widetilde{\boldsymbol{U}}(\boldsymbol{x})$, for which $\mathbf{J} = \mathbf{curl}\,\mathbf{H_s}$ and the assumptions of the theorem hold. In both experiments $\boldsymbol{u}$ is linear in $t$ and the scheme is modified as above, so the right-hand side of the error equation reduces to the face terms, and the proof of Theorem 11 applies, also to the source of Example 2, without Lemma 5. Again, when $\Delta t$ goes from 0.1 to 0.05 the errors change by less than 0.2% (by 1.6% for $E_\varphi$). Table 7 shows the results for $k = 2$ and $\Delta t = 0.05$. All the errors converge with order close to $3 = k+1$; in particular, the orders of $E_{\boldsymbol{u}}$ and $E_{\boldsymbol{z}}$, which could not be measured in Example 1 because of the time discretization error, are 2.81, 2.92, 2.96 and 2.93, 2.97, 2.99, respectively, above the rate $h^{5/2}$ of Theorem 11. The discrete flux on $\Gamma_0$ was below $4 \times 10^{-15}$ in all the runs.

Table 7: Example 3 with the function $\widetilde{\psi}$ of Example 1 ($g(t) = 1 + t$, $\mathbf{J} = \mathbf{curl}\,\mathbf{H_s}$, no time discretization error): errors and orders of convergence in $h$ for $\Delta t = 0.05$.

| | mesh | $h$ | $E_{\boldsymbol{u}}$ | $r_h$ | $E_{\boldsymbol{z}}$ | $r_h$ | $E_\varphi$ | $r_h$ |
|---|---|---|---|---|---|---|---|---|
| $k = 2$ | 1 | 0.3464 | 8.95e-02 | – | 2.16e-02 | – | 6.11e-02 | – |
| | 2 | 0.1732 | 1.28e-02 | 2.81 | 2.83e-03 | 2.93 | 7.62e-03 | 3.00 |
| | 3 | 0.1155 | 3.90e-03 | 2.92 | 8.47e-04 | 2.97 | 2.35e-03 | 2.90 |
| | 4 | 0.0866 | 1.67e-03 | 2.96 | 3.59e-04 | 2.99 | 1.02e-03 | 2.89 |

Summarizing, the experiments are consistent with Theorem 11 and Remark 13: the scheme is of first order in $\Delta t$, and the spatial part of the error decreases at least with order $k + 1/2$. In fact, the observed order in $h$ is close to $k + 1$ for $k = 1, 2$, and for $k = 0$ it approaches or exceeds 1 as the mesh is refined, which, on the structured meshes used here, suggests that the loss of $h^{1/2}$ in (35) is due to the analysis (see the remark on the loss of $h^{1/2}$ after Theorem 11).

### 5.4 Example 4: magnetic shielding by eddy currents

We now consider a configuration of physical interest, with no current source ($\mathbf{J} = \mathbf{0}$), in which the conductor is exposed to an external magnetic field that is switched on at $t = 0$:

$$\mathbf{H}_a(t) = H_a(t)\,\boldsymbol{e}_z, \qquad H_a(t) = H_0\big(1 - e^{-t/t_r}\big), \qquad H_0 = 1, \quad t_r = 0.02.$$

In vacuum, this uniform field is generated by the vector potential $\boldsymbol{A}_a(t,\boldsymbol{x}) = \frac{\mu}{2} H_a(t)\big(-(y-\frac{1}{2}),\, x-\frac{1}{2},\, 0\big)$, with $\mathbf{curl}\,\boldsymbol{A}_a = \mu\mathbf{H}_a$, and the associated electric field is $\mathbf{E}_a = -\partial_t \boldsymbol{A}_a$. The field is applied through the boundary condition on $\Gamma$, with datum

$$\boldsymbol{g}^m = \boldsymbol{n} \times \big(-\overline{\partial}_t \boldsymbol{A}_a^m\big), \qquad m = 1, \ldots, M.$$

This discrete datum is consistent with the treatment of the source in (7): with it, the magnetic flux entering through $\Gamma$ between $t_0$ and $t_m$ coincides exactly with that of $\mathbf{H}_a(t_m)$. If $\boldsymbol{g}^m$ is instead evaluated pointwise as $\boldsymbol{n} \times \mathbf{E}_a(t_m)$, part of the applied flux is lost in the first steps (where $H_a$ varies rapidly compared with $\Delta t$), and the field inside the conductor stabilizes at about $0.77\,H_0$ instead of $H_0$; this value is precisely the right-endpoint rectangle rule $\Delta t \sum_{m\geq 1} H_a'(t_m) = \frac{\Delta t}{t_r}\,\frac{e^{-\Delta t/t_r}}{1-e^{-\Delta t/t_r}} H_0 \approx 0.771\,H_0$ for $\Delta t = 0.01$.

Initially $\boldsymbol{u}_0 = \mathbf{0}$. Since $\mu\partial_t \mathbf{H} = -\,\mathbf{curl}\,\mathbf{E}$ and $\boldsymbol{z} = \mu^{-1}\,\mathbf{curl}\,\boldsymbol{u}$, the magnetic field is recovered from the HDG solution by

$$\mathbf{H}_h^0 = \mathbf{0}, \qquad \mathbf{H}_h^m = \mathbf{H}_h^{m-1} - \Delta t\,\boldsymbol{z}_h^m, \qquad m = 1, \ldots, M,$$

and we also compute the induced current density $\mathbf{J}_{\mathsf{e}} := \sigma \boldsymbol{u}_h^m$ and the Joule power $P(t_m) := \|\sqrt{\sigma}\,\boldsymbol{u}_h^m\|^2_{\mathcal{T}_h^c}$. We take $k = 1$, $\Delta t = 0.01$ and $T = 1$.

When the external field is switched on, the currents induced in the conductor oppose the variation of the magnetic flux (Lenz's law), so that the field enters the conductor with a delay. Inside the conductor, $\mathbf{H}$ satisfies $\partial_t \mathbf{H} = (\mu\sigma)^{-1}\,\triangle\mathbf{H}$, and the delay is governed by a diffusion time which, for a cube of side $L$ with $\mathbf{H} = \mathbf{H}_a$ on its surface, is $\tau = \mu\sigma L^2/(3\pi^2)$, the inverse of the first Dirichlet eigenvalue of $-(\mu\sigma)^{-1}\triangle$. For $L = 0.6$ this gives $\tau \approx 0.1216$. This value is only an estimate here, since the field on $\Gamma_0$ is not prescribed but results from the coupling with $\Omega_{\mathtt{d}}$.

Figure 1 shows the evolution of the vertical component of $\mathbf{H}_h$ at the center $\boldsymbol{x}_c = (\frac{1}{2}, \frac{1}{2}, \frac{1}{2})$ of the conductor for meshes 1 to 4. When the applied field has practically reached its final value ($t \approx 0.1$), the field at the center is still below 20% of $H_0$ on meshes 2 to 4; after the first steps it increases monotonically and reaches 99.9% of $H_0$ at $t = 1$ on meshes 3 and 4. On mesh 1 the field at the center becomes slightly negative in the first steps (down to $-0.06\,H_0$), which is not physical; this artifact is reduced under refinement (below $0.003\,H_0$ in absolute value on mesh 2), and the curves of meshes 2 to 4 are almost indistinguishable. Table 8 lists several quantities of interest. Between meshes 3 and 4, the field at the center changes by about 1% for $t \geq 0.21$ (by 4% at $t = 0.11$, where it is small), the time at which it reaches 63% of $H_0$ does not change, and the Joule power changes by less than 0.5% for $t \leq 0.21$ (the relative changes are larger in the tail, where $P$ is several orders of magnitude smaller). The diffusion time $\tau_h$, obtained by a least-squares fit of $H_0 - H_{h,z}(t,\boldsymbol{x}_c) \approx C\,e^{-t/\tau_h}$ on the interval $[0.3\,t^*, t^*]$, where $t^*$ is the last time with $H_0 - H_{h,z}(t,\boldsymbol{x}_c) > 10^{-3} H_0$, decreases under refinement and, on mesh 4, differs from the estimate $\tau$ by 1.4%. We note that $\tau_h$ is less accurate than the other quantities, since it is obtained from the tail of the solution, where $H_0 - H_{h,z}$ is small.

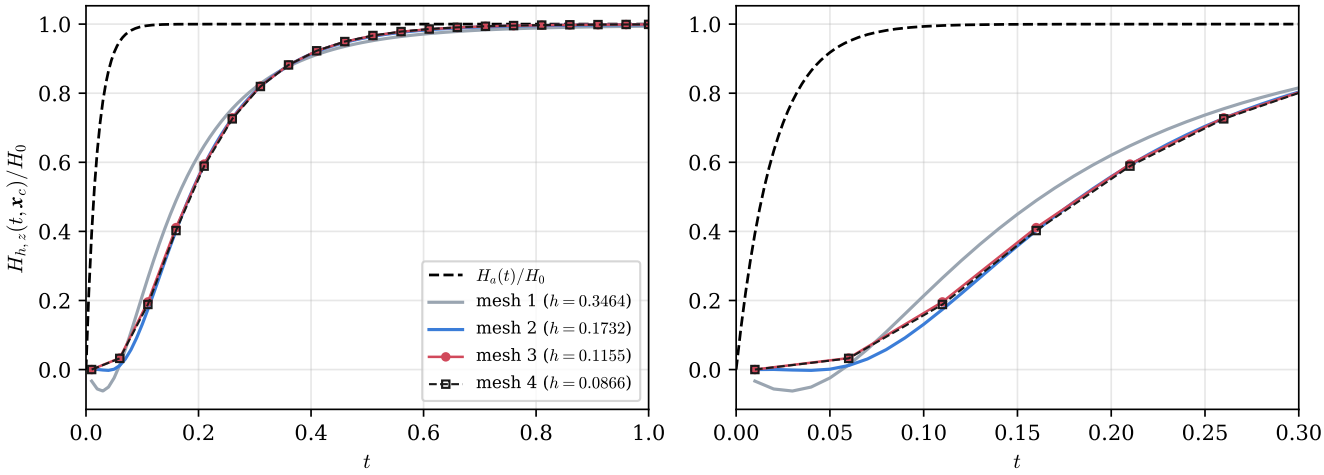



Figure 1: Magnetic shielding: vertical component of $\mathbf{H}_h$ at the center of the conductor, compared with the applied field, for meshes 1 to 4 ($k = 1$, $\Delta t = 0.01$). Right: detail for $0 \le t \le 0.3$

Table 8: Magnetic shielding: quantities of interest for meshes 1 to 4 ($k = 1$, $\Delta t = 0.01$).

| | Mesh 1 | Mesh 2 | Mesh 3 | Mesh 4 |
|---|---|---|---|---|
| $H_{h,z}(0.11, \boldsymbol{x}_c)/H_0$ | 0.265 | 0.174 | 0.196 | 0.188 |
| $H_{h,z}(0.21, \boldsymbol{x}_c)/H_0$ | 0.648 | 0.592 | 0.595 | 0.589 |
| $H_{h,z}(1, \boldsymbol{x}_c)/H_0$ | 0.9939 | 0.9982 | 0.9989 | 0.9992 |
| time at which $H_{h,z}(t, \boldsymbol{x}_c) = 0.63\, H_0$ | 0.21 | 0.23 | 0.23 | 0.23 |
| diffusion time $\tau_h$ ($\tau \approx 0.1216$) | 0.2048 | 0.1444 | 0.1309 | 0.1233 |
| $P(0.06)$ | 0.915 | 1.040 | 1.052 | 1.052 |
| $P(0.21)$ | 0.0771 | 0.0694 | 0.0683 | 0.0680 |
| $\max_m \lVert\varphi_h^m\rVert_{\mathcal{T}_h^d}$ | $1.37 \times 10^{-1}$ | $8.54 \times 10^{-2}$ | $6.51 \times 10^{-2}$ | $5.44 \times 10^{-2}$ |
| $\lVert\varphi_h^M\rVert_{\mathcal{T}_h^d}$ | $1.17 \times 10^{-3}$ | $6.06 \times 10^{-4}$ | $3.70 \times 10^{-4}$ | $2.62 \times 10^{-4}$ |
| $\max_m$ discrete flux on $\Gamma_0$ | $2.6 \times 10^{-15}$ | $2.5 \times 10^{-16}$ | $2.3 \times 10^{-15}$ | $1.2 \times 10^{-15}$ |

The spatial distribution of the solution on mesh 4 is shown in Figures 2 and 3 (elementwise averages). At $t = 0.02$ the field is expelled from the conductor and concentrates in the dielectric between the conductor and the outer boundary, where it reaches about $1.4\, H_a$. This concentration is enhanced by the outer boundary: the boundary condition on $\Gamma$ fixes the magnetic flux through $\Gamma$, so that the flux expelled from the conductor has to cross the dielectric (if the whole field were expelled, the mean field in the dielectric on a horizontal section would be $H_a/(1 - 0.36) \approx 1.56\, H_a$); for a conductor in free space, the field around it would be less concentrated. The induced currents are confined to a thin layer near the surface of the conductor. As time increases, the field penetrates from the faces of the conductor towards its center, the currents move to the interior and decay, and at $t = 1$ the field is again uniform. Figure 3 shows that the induced currents circulate around the $z$-axis in the direction that generates a magnetic field opposite to $\mathbf{H}_a$, as predicted by Lenz's law.

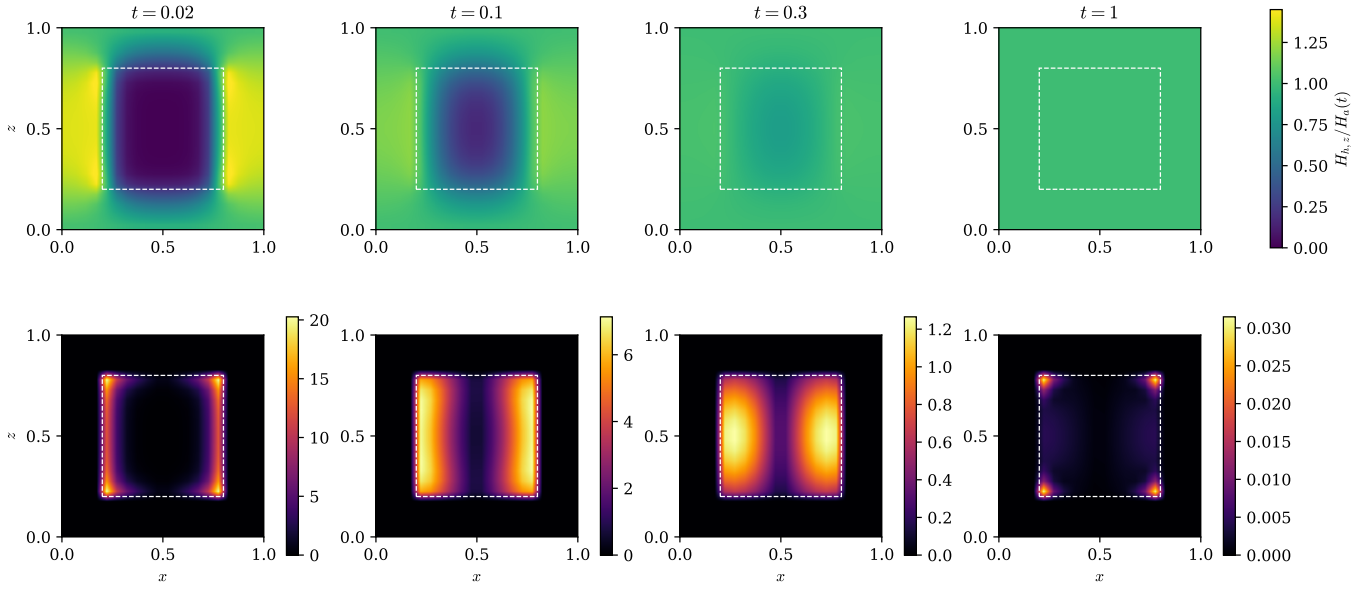



Figure 2: Magnetic shielding, mesh 4: vertical cut $y = \frac{1}{2}$. Top: $H_{h,z}/H_a(t)$. Bottom: $|\mathbf{J_e}|$. The dashed line is the boundary of the conductor

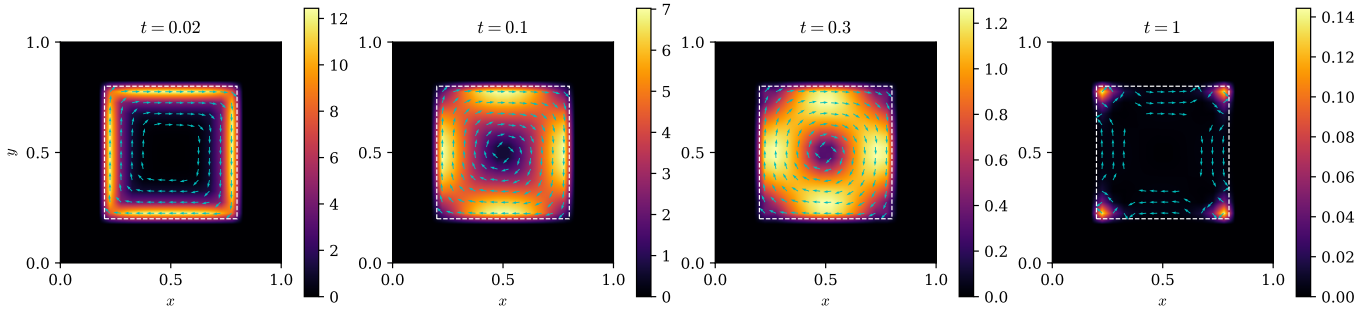



Figure 3: Magnetic shielding, mesh 4: horizontal cut $z = \frac{1}{2}$. Color: $|\mathbf{J_e}|$; arrows: direction of $\mathbf{J_e}$

Finally, the discrete flux on $\Gamma_0$ vanishes up to round-off for all the meshes, and $\varphi_h$ tends to zero under refinement (Table 8), in agreement with Proposition 2. The rate is lower than for $k = 1$ in Examples 1 and 2 (about 1 for $\left\|\varphi_h^M\right\|_{\mathcal{T}_h^d}$): in this problem the solution is not smooth near the edges and corners of $\Omega_{\mathtt{c}}$, which are reentrant for $\Omega_{\mathtt{d}}$; in particular, the regularity assumed in Theorem 11 does not hold here, and the theorem does not predict the rates for this problem, although all the computed quantities converge under refinement. The abrupt switching of the applied field also produces the large values of $\varphi_h$ in the first time step. The residual currents at $t = 1$ are also concentrated near the vertical edges of the conductor (Figure 3).

# 6 Conclusions

We have proposed and analyzed a fully discrete HDG method for the transient eddy current problem in terms of the electric field, in a domain composed of a conductor and a dielectric region. A Lagrange multiplier imposes the divergence-free condition in the dielectric, and the charge condition on the interface adds a single global scalar unknown. We proved that the scheme is well posed and stable, and that the error is of order $\mathcal{O}(h^{k+1/2} + \Delta t)$ for the electric field in the conductor, for the variable $\boldsymbol{z}$, and for the multiplier. To the best of our knowledge, these are the first error estimates for an HDG method applied to the transient eddy current problem.

In the experiments with manufactured solutions, the scheme is of first order in $\Delta t$ when the temporal part of the error dominates, and the spatial order exceeds $k + 1/2$. It is close to $k + 1$ for $k = 1, 2$, and it approaches or exceeds 1 for $k = 0$. On the structured meshes used here, this suggests that the estimate is not sharp. Similar orders are observed for a source whose normal component jumps across the interface, a case covered by Remark 13. In Example 4 we notice that the regularity assumed in Theorem 11 fails. The computed quantities are still reasonable under mesh refinement, and the method reproduces the delay of the field inside the conductor due to the induced currents and its subsequent diffusion.

# Declarations

**Funding** R. Acevedo has been partially supported by Universidad del Cauca, through project VRI ID 6779. C. Gómez has been partially supported by Universidad de los Llanos, through project DGI C07-02-2025-017.

**Acknowledgements** R. Bustinza would like to thank Universidad de los Llanos, Villavicencio, Colombia, for their hospitality during his stay in October 2026.

**Competing interests** The authors declare no competing interests.

**Ethics approval** Not applicable.

**Consent to participate** Not applicable.

**Consent for publication** Not applicable.

**Data availability** The data generated in this study and the MATLAB code are available from the authors on reasonable request.

**Materials availability** Not applicable.

**Code availability** The data generated in this study and the MATLAB code are available from the authors on reasonable request.

**Author contribution** All authors contributed equally to this work.

## References


[1] Acevedo, R., Arias, C., Gómez, C.: Optimal convergence analysis for a FEM approximation of a transient eddy current problem incorporating velocity terms. Results in Applied Mathematics **23**, 100478 (2024). https://doi.org/10.1016/j.rinam.2024.100478

[2] Acevedo, R., Bustinza, R., Gómez, C.: A transient eddy current problem via potential formulation with current excitation. Preprint 2025-11, Centro de Investigación en Ingeniería Matemática, Universidad de Concepción, Chile (2025). URL `https://www.ci2ma.udec.cl/pdf/pre-publicaciones2/2025/pp25-11.pdf`

[3] Acevedo, R., Gómez, C., López-Rodríguez, B.: Fully discrete finite element approximation for a family of degenerate parabolic mixed equations. Computers & Mathematics with Applications **96**, 155–177 (2021). https://doi.org/10.1016/j.camwa.2021.05.010

[4] Acevedo, R., Meddahi, S.: An $E$-based mixed FEM and BEM coupling for a time-dependent eddy current problem. IMA Journal of Numerical Analysis **31**(2), 667–697 (2011). https://doi.org/10.1093/imanum/drp049

[5] Acevedo, R., Meddahi, S., Rodríguez, R.: An $E$-based mixed formulation for a time-dependent eddy current problem. Mathematics of Computation **78**(268), 1929–1949 (2009). https://doi.org/10.1090/S0025-5718-09-02254-6

[6] Alonso Rodríguez, A., Márquez, A., Meddahi, S., Valli, A.: A discontinuous Galerkin method for a time-harmonic eddy current problem. Calcolo **55**(3), 25 (2018). https://doi.org/10.1007/s10092-018-0267-2

[7] Alonso Rodríguez, A., Valli, A.: Eddy Current Approximation of Maxwell Equations: Theory, Algorithms and Applications, *MS&A. Modeling, Simulation and Applications*, vol. 4. Springer-Verlag Italia, Milan (2010). https://doi.org/10.1007/978-88-470-1506-7

[8] Ammari, H., Buffa, A., Nédélec, J.C.: A justification of eddy currents model for the Maxwell equations. SIAM Journal on Applied Mathematics **60**(5), 1805–1823 (2000). https://doi.org/10.1137/S0036139998348979

[9] Amrouche, C., Bernardi, C., Dauge, M., Girault, V.: Vector potentials in three-dimensional non-smooth domains. Mathematical Methods in the Applied Sciences **21**(9), 823–864 (1998). https://doi.org/10.1002/(SICI)1099-1476(199806)21:9<823::AID-MMA976>3.0.CO;2-B

[10] Berardocco, L., Kronbichler, M., Gravemeier, V.: A hybridizable discontinuous Galerkin method for electromagnetics with a view on subsurface applications. Computer Methods in Applied Mechanics and Engineering **366**, 113071 (2020). https://doi.org/10.1016/j.cma.2020.113071

[11] Bermúdez, A., Gómez, D., Salgado, P.: Mathematical Models and Numerical Simulation in Electromagnetism, *UNITEXT*, vol. 74. Springer, Cham (2014). https://doi.org/10.1007/978-3-319-02949-8

[12] Bermúdez, A., López-Rodríguez, B., Rodríguez, R., Salgado, P.: Numerical solution of transient eddy current problems with input current intensities as boundary data. IMA Journal of Numerical Analysis **32**(3), 1001–1029 (2012). https://doi.org/10.1093/imanum/drr028

[13] Bossavit, A.: Computational Electromagnetism. Academic Press, San Diego, CA (1998). https://doi.org/10.1016/B978-0-12-118710-1.X5000-4

[14] Bustinza, R., López-Rodríguez, B., Osorio, M.: An a priori error analysis of an HDG method for an eddy current problem. Mathematical Methods in the Applied Sciences **41**(7), 2795–2810 (2018). https://doi.org/10.1002/mma.4780

[15] Chabaud, B., Cockburn, B.: Uniform-in-time superconvergence of HDG methods for the heat equation. Mathematics of Computation **81**(277), 107–129 (2012). https://doi.org/10.1090/S0025-5718-2011-02525-1

[16] Chen, H., Qiu, W., Shi, K., Solano, M.: A superconvergent HDG method for the Maxwell equations. Journal of Scientific Computing **70**(3), 1010–1029 (2017). https://doi.org/10.1007/s10915-016-0272-z

[17] Christophe, A., Descombes, S., Lanteri, S.: An implicit hybridized discontinuous Galerkin method for the 3D time-domain Maxwell equations. Applied Mathematics and Computation **319**, 395–408 (2018). https://doi.org/10.1016/j.amc.2017.04.023

[18] Ciarlet, P.G.: The Finite Element Method for Elliptic Problems, *Studies in Mathematics and its Applications*, vol. 4. North-Holland, Amsterdam (1978). https://doi.org/10.1016/S0168-2024(08)X7014-6

[19] Cockburn, B., Du, S., Sánchez, M.A.: *A priori* error analysis of new semidiscrete, Hamiltonian HDG methods for the time-dependent Maxwell's equations. ESAIM: Mathematical Modelling and Numerical Analysis **57**(4), 2097–2129 (2023). https://doi.org/10.1051/m2an/2023048

[20] Cockburn, B., Gopalakrishnan, J., Lazarov, R.: Unified hybridization of discontinuous Galerkin, mixed, and continuous Galerkin methods for second order elliptic problems. SIAM Journal on Numerical Analysis **47**(2), 1319–1365 (2009). https://doi.org/10.1137/070706616

[21] Cockburn, B., Gopalakrishnan, J., Sayas, F.J.: A projection-based error analysis of HDG methods. Mathematics of Computation **79**(271), 1351–1367 (2010). https://doi.org/10.1090/S0025-5718-10-02334-3

[22] Di Pietro, D.A., Ern, A.: Mathematical Aspects of Discontinuous Galerkin Methods, *Mathématiques et Applications*, vol. 69. Springer, Berlin, Heidelberg (2012). https://doi.org/10.1007/978-3-642-22980-0

[23] Du, S., Sayas, F.J.: A unified error analysis of hybridizable discontinuous Galerkin methods for the static Maxwell equations. SIAM Journal on Numerical Analysis **58**(2), 1367–1391 (2020). https://doi.org/10.1137/19m1290966

[24] Heywood, J.G., Rannacher, R.: Finite-element approximation of the nonstationary Navier–Stokes problem. Part IV: Error analysis for second-order time discretization. SIAM Journal on Numerical Analysis **27**(2), 353–384 (1990). https://doi.org/10.1137/0727022

[25] Lee, J.J.: A hybridizable discontinuous Galerkin method for time-modulated Drude–Lorentz media (2026). https://doi.org/10.48550/arXiv.2610.21991. Preprint, arXiv:2610.21991

[26] Meddahi, S., Selgas, V.: An $H$-based FEM-BEM formulation for a time dependent eddy current problem. Applied Numerical Mathematics **58**(8), 1061–1083 (2008). https://doi.org/10.1016/j.apnum.2007.04.002

[27] Nguyen, N.C., Peraire, J., Cockburn, B.: Hybridizable discontinuous Galerkin methods for the time-harmonic Maxwell's equations. Journal of Computational Physics **230**(19), 7151–7175 (2011). https://doi.org/10.1016/j.jcp.2011.05.018

[28] Perugia, I., Schötzau, D.: The $hp$-local discontinuous Galerkin method for low-frequency time-harmonic Maxwell equations. Mathematics of Computation **72**(243), 1179–1214 (2003). https://doi.org/10.1090/S0025-5718-02-01471-0

[29] Pi, W., Han, Y., Zhang, S.: A hybridisable discontinuous Galerkin method for time-dependent convection-diffusion-reaction equations. East Asian Journal on Applied Mathematics **10**(3), 455–484 (2020). https://doi.org/10.4208/eajam.090419.041219

[30] Quarteroni, A., Valli, A.: Numerical Approximation of Partial Differential Equations, *Springer Series in Computational Mathematics*, vol. 23. Springer, Berlin (2008). https://doi.org/10.1007/978-3-540-85268-1. First softcover printing of the 1994 edition

[31] Šebestová, I.: Residual-based a posteriori error estimation for $E$-based formulation of a time-dependent eddy current problem. Computers & Mathematics with Applications **174**, 204–218 (2024). https://doi.org/10.1016/j.camwa.2024.08.020

[32] Zheng, W., Chen, Z., Wang, L.: An adaptive finite element method for the **H**-$\psi$ formulation of time-dependent eddy current problems. Numerische Mathematik **103**(4), 667–689 (2006). https://doi.org/10.1007/s00211-006-0008-3

# Centro de Investigación en Ingeniería Matemática (CI$^2$MA)

## PRE-PUBLICACIONES 2026

2026-25 Fernando Muñoz García, Fernando Roldán: *Forward-reflected-backward algorithm with linesearch*

2026-26 Eider Aldana, Ricardo Oyarzúa: *A Lagrange multiplier approach for fluid-flow problem with inhomogeneous mixed boundary conditions*

2026-27 Jean-Christophe Pesquet, Fernando Roldán: *Nonlinear forward-backward algorithm for solving non-monotone+Lipschitz inclusions with applications to adjoint mismatch problems*

2026-28 Juan Barajas-Calonge, Julio Careaga, Luis M. Villada: *Invariant-region-preserving high-order schemes for a model of reactive sedimentation*

2026-29 Aníbal Coronel, Fernando Huancas, Mauricio Sepúlveda: *Theoretical analysis and numerical validation of an inverse problem in a SIS reaction–diffusion system, Part 1: Identification of transmission and recovery rates*

2026-30 Rodrigo Carrasco Jofré, Mauricio Sepúlveda, Jaime Muñoz-Rivera: *Analytic and Gevrey regularity for a hybrid thermoelastic Euler–Bernoulli beam with singular interactions*

2026-31 Gabriel N. Gatica: *A note on arbitrarily small solenoidal liftings of Dirichlet data*

2026-32 Juan Barajas-Calonge, Raimund Bürger, Pep Mulet, Luis M. Villada: *An invariant-region-preserving finite-volume-element scheme for a polydisperse model of flow and segregation in general domains*

2026-33 Eider Aldana, Ricardo Oyarzúa: *A Lagrange multiplier-based finite element method for a reverse osmosis model*

2026-34 Gonzalo A. Benavides, Sergio Caucao, Gabriel N. Gatica: *New skew-symmetry-based mixed finite element methods for the Navier-Stokes equations with variable viscosity*

2026-35 Isaac Bermudez, Jaime Manríquez, Manuel Solano: *Analysis of an unfitted HDG method for the coupled linear elasticity/Stokes problema*

2026-36 Ramiro Acevedo, Rommel Bustinza, Christian Gómez: *A hybridizable discontinuous Galerkin method for the time-dependent eddy current problem in an electric field formulation*

Para obtener copias de las Pre-Publicaciones, escribir o llamar a: Director, Centro de Investigación en Ingeniería Matemática, Universidad de Concepción, Casilla 160-C, Concepción, Chile, Tel.: 41-2661324, o bien, visitar la página web del centro: `http://www.ci2ma.udec.cl`








Centro de Investigación en
Ingeniería Matemática (CI²MA)
**Universidad de Concepción**

Casilla 160-C, Concepción, Chile
Tel.: 56-41-2661324/2661554/2661316
http://www.ci2ma.udec.cl

